Validating V_{S30}-based site amplification factors in hybrid broadband ground-motion simulation of small-magnitude earthquakes in New Zealand

Journal Title
XX(X):3–

DOI: 10.1177/ToBeAssigned

Felipe Kuncar [1], Brendon A. Bradley[1], Christopher A. de la Torre[1]

Prepared using sagej.cls

Abstract

V_{S30}-based site amplification factors are commonly used to account for local site effects in hybrid broadband ground-motion simulation when site-specific data are limited. Validation against observations allows for testing alternative semi-empirical V_{S30}-based models and establishing proper protocols for their application in forward analyses. This article validates alternative implementations of V_{S30}-based site factors using 5218 ground motions from 479 small-magnitude events recorded at 212 sites in New Zealand, which represent a wide range of site conditions. The investigation of (Fourier) effective amplitude spectra (EAS) residuals allows for a direct assessment of the low-frequency (LF; $f < 1$ Hz) and high-frequency (HF; $f > 1$ Hz) components of the hybrid broadband simulation approach, and the corresponding effect of the site 'adjustment'. Before applying the site factor, the LF simulation exhibits systematic underprediction and the HF simulation displays systematic overprediction. The use of site factors based on semi-empirical models for EAS, developed in the last decade, results in comparable, or slightly better, prediction performance compared to response spectra-based models commonly used in previous validation studies. A greater LF underprediction was identified at sites located within sedimentary basins that are less constrained by site data or not properly modeled in the LF simulation due to limitations in spatial discretization. A simple protocol is proposed for the application of the LF site factor based on a basin-type and geomorphic site categorization, which reduces the variability of EAS prediction residuals by up to 0.1 natural log units. The explicit incorporation of the parameter $Z_{1.0}$, or alternatively, the use of a host-to-target correction factor demonstrates that a significant portion of the HF systematic overamplification in the frequency range 1.0-3.0 Hz can be explained by V_S profile features not accounted for by V_{S30} alone. These findings can inform the application of site adjustments in future studies and guide advancements in the LF and HF simulation components.

Keywords

Site effects, site factor, V_{S30}, hybrid broadband ground-motion simulation, ground-motion prediction, validation, New Zealand

Introduction

Proper modeling of near-surface site effects is key for improving the predictive capabilities of hybrid broadband ground-motion simulation. This simulation method utilizes two different approaches for the modeling of low frequencies (LFs) and high frequencies (HFs), and produces broadband (BB) ground-motion time series for use in engineering applications (Baker et al. 2021, Ch. 5). Due to computational constraints and knowledge limitations of near-surface material properties, site effects are only partially accounted for in the LF and HF simulations (Kuncar et al. 2025a), and hence, the simulated waveforms require posterior adjustments, which can be performed via site factors applied in the Fourier spectral domain (e.g., Graves and Pitarka 2010; Razafindrakoto et al. 2018; Lee et al. 2022). These site factors (SFs) can be based on a variety of site-response approaches and include a range of site-characterization data (Kuncar et al. 2025a). In some applications, including regional simulation-based probabilistic seismic hazard analysis (e.g., Graves et al. 2011; Bradley 2020), site-specific characterization data are not available at all locations of interest. In these situations, the 30-m time-averaged shear-wave velocity, V_{S30}, which can be obtained from regional V_{S30} maps based on surface geology, topographic slope, and V_S measurements (e.g., Foster et al. 2019; Geyin and Maurer 2023), is typically used to characterize the site conditions. Given V_{S30}, the V_{S30}-based site-response scaling factor of a semi-empirical ground-motion model (GMM) can be used to derive the SF to be applied to simulations (e.g., Graves and Pitarka 2010; Rodgers et al. 2020; Lee et al. 2022; Kuncar et al. 2025a; Matinrad and Petrone 2025). In addition to V_{S30}, the SF can also consider additional site parameters, such as the depth to a V_S of 1 km/s, $Z_{1.0}$.

To assess the predictive capability of hybrid broadband ground-motion simulation and V_{S30}-based SFs in capturing site effects, validation against observations using multiple sites and events is needed (Bradley et al. 2017a; Rezaeian et al. 2024). Several such studies have been carried out in different regions, using varying amounts of validation

[1]Civil and Environmental Engineering, University of Canterbury, Christchurch, New Zealand

Corresponding author:
Felipe Kuncar
Private Bag 4800, Christchurch 8140, New Zealand
Email: felipe.kuncar@canterbury.ac.nz

Prepared using sagej.cls

data and different GMMs to determine the site factor (e.g., Graves and Pitarka 2010; Galasso et al. 2012; Iwaki et al. 2016; Razafindrakoto et al. 2018; de la Torre et al. 2020; Lee et al. 2020; Razafindrakoto et al. 2021; Lee et al. 2022; Graves 2022; Kuncar et al. 2025b). In New Zealand (NZ), Lee et al. (2022) used 5218 ground motions from 479 small-magnitude earthquakes recorded at 212 sites, representing the largest validation dataset considered to date globally (to the best of the authors' knowledge). Lee et al. (2022) considered the Campbell and Bozorgnia (2014) (CB14) model for pseudo-spectral acceleration (SA) to determine the site factor. Based on previous validation studies that identified significant overprediction at long vibration periods when the SF was applied to the LF simulation component (Lee et al. 2020; de la Torre et al. 2020), the SF was only applied to the HF simulation component (i.e., $f > 1$ Hz). As explained in Lee et al. (2022), since the LF simulation was produced using a 3D velocity model, the application of the SF to this component in previous studies was likely double-counting LF site effects. Furthermore, Kuncar et al. (2025a) identified that a systematic inconsistency between the V_S profile implicit in the CB14 model (following the approach of Al Atik and Abrahamson 2021) and the corresponding V_S profile in the LF simulation tends to further increase this overprediction.

Despite the significant progress towards simulation validation that has occurred in the last decade (e.g., Rezaeian et al. 2024), several limitations in Lee et al. (2022) and other prior studies still need to be addressed, particularly regarding the modeling of site effects. Specifically:

(1) Lee et al. (2022) was limited to only one SF (based on one GMM), which does not account for the epistemic uncertainty in the selection of alternative site response models (Lee et al. 2024; Baker et al. 2021, Ch. 4). Furthermore, since the SF is applied in the Fourier spectral domain, the use of a SA-based GMM (such as the CB14 model) is problematic due to the differences in scaling between SA and Fourier amplitude spectra (FAS) (Bora et al. 2016; Stafford et al. 2017). To mitigate this inconsistency, Lee et al. (2022) and other studies (e.g., Razafindrakoto et al. 2021) have considered a heuristic truncation of the SF to $SF = 1$ at high frequencies, but this is still inconsistent with the high-frequency attenuation that site response should produce (Baker et al. 2021, Ch. 5). In recent years, GMMs and site-response models have been developed for FAS and EAS (effective amplitude spectra, corresponding to the orientation-independent horizontal-component of FAS) (e.g., Bayless and Abrahamson 2019; Bora et al. 2019; Shi 2019; Campbell and Bozorgnia 2025), which can be utilized to derive more consistent SFs. Several studies have already used (e.g., Rodgers et al. 2020; Matinrad and Petrone 2025)

or validated (e.g., Razafindrakoto et al. 2021; Kuncar et al. 2025b) such FAS-based models, but for a significantly smaller number of sites and events than those considered in Lee et al. (2022), and/or for other regions and simulation approaches.

(2) Prior validation studies in NZ (e.g., Razafindrakoto et al. 2018; de la Torre et al. 2020; Lee et al. 2020, 2022; Kuncar et al. 2025b) have focused on intensity measures (IMs) commonly used in engineering applications, such as pseudo-spectral acceleration (SA). However, a more robust evaluation of simulation predictions also requires considering FAS, which directly represents the ground motion at each frequency and allows for the separate, and more transparent, assessment of the LF and HF simulations, and the corresponding effect of the site adjustment.

(3) The application of the SF to the HF simulation component only, considered in Lee et al. (2022), requires further examination. This factor should not be required for the LF simulation in concept; however, limitations in the quality of the 3D velocity model and the spatial discretization adopted in the numerical wave-propagation computation may result in the need to add some extra level of amplification in this frequency range. Since the quality and characteristics of a 3D velocity model differ across a region (NZ in this context), the frequency range of application of the site factor should also vary, and this needs to be evaluated through validation.

(4) Given that a range of different sites can be represented by the same V_{S30} value, using only V_{S30} to determine SF (such as in Lee et al. 2022) is a major limitation. Even if site-specific data (e.g., a measured V_S profile) are not available at one particular location, complementary site parameters (e.g., inferred $Z_{1.0}$) can be considered along with V_{S30} to constrain the SF. Similarly, the information of the V_S profile represented in the simulation and that implicit in the GMM (the so-called, host profile) can be used, in addition to V_{S30}, to adjust the site factor to be more consistent with the simulation conditions. A host-to-target adjustment of this type was proposed by Kuncar et al. (2025a), but has not yet been validated against observations.

This article presents a comprehensive validation study of alternative implementations of the V_{S30}-based site factor for hybrid broadband ground-motion simulation in NZ, considering the 212 sites and 479 small-magnitude ($3.5 \leq M_W \leq 5.0$) events included in Lee et al. (2022). The layout of the paper is as follows: first, observational and site data are presented. Second, simulation and validation methodologies are described, along with the alternative SF models considered. Lastly, validation results are presented, covering the four different aspects discussed above: (1) use of alternative GMMs, including EAS-based models; (2) examination of EAS residuals and their relationship with SA residuals;

(3) evaluation of the frequency range of the SF application; and (4) consideration of additional information to constrain the site factor, including $Z_{1.0}$, and the host and simulation profiles.

Data and site characterization

Stations, earthquakes, and observed ground motions

This study utilizes the observational ground-motion database of active shallow crustal earthquakes with magnitude $3.5 \leq M_W \leq 5.0$ developed by Lee et al. (2022). Similar to Lee et al. (2022), only stations and events with at least three high-quality ground-motion recordings were included. Ground-motion quality was assessed using the quality classification neural network of Bellagamba et al. (2019). The threshold of three recordings was chosen to limit the influence of potential statistical outliers while maintaining a sufficient number of stations and events for the validation study. This resulted in 5218 ground motions from 479 events recorded at 212 sites. Figure 1 presents the spatial distribution of the sites and earthquake sources considered across NZ. Figure 2 shows the distribution of observed ground motions in terms of peak ground acceleration (PGA) versus magnitude and V_{S30}. Although most of the observed PGA values are relatively low (implying limited soil nonlinearity), there are several stations with $V_{S30} < 300$ m/s that recorded $PGA > 0.1g$, which may result in considerable levels of soil nonlinearity (e.g., Kaklamanos et al. 2013).

Velocity model and basin type classification

As subsequently explained in the "Ground-motion simulation method" section, the LF component of the ground-motion simulations used in this study (Lee et al. 2022) were produced utilizing the NZ Velocity model (NZVM, Thomson et al. 2020) v2.02. This model is based on the NZ-wide travel-time tomography model of Eberhart-Phillips et al. (2010) along with multiple embedded subregions, representing different sedimentary basins across the country. Thomson et al. (2020) classified these subregions into four types (Types 1 to 4), reflecting increasing levels of site characterisation used for the basin models. Type 1 relies on the slope at rock outcrops, geologic maps, and cross sections; Type 2 incorporates some direct measurements to infer basin surface depth; Type 3 includes velocity-profile information; and Type 4 corresponds to an arbitrarily complex basin model. In this study (based on NZVM v2.02), Canterbury is classified as a Type 4 subregion. It uses a comprehensive basin model (Lee et al. 2017) that integrates

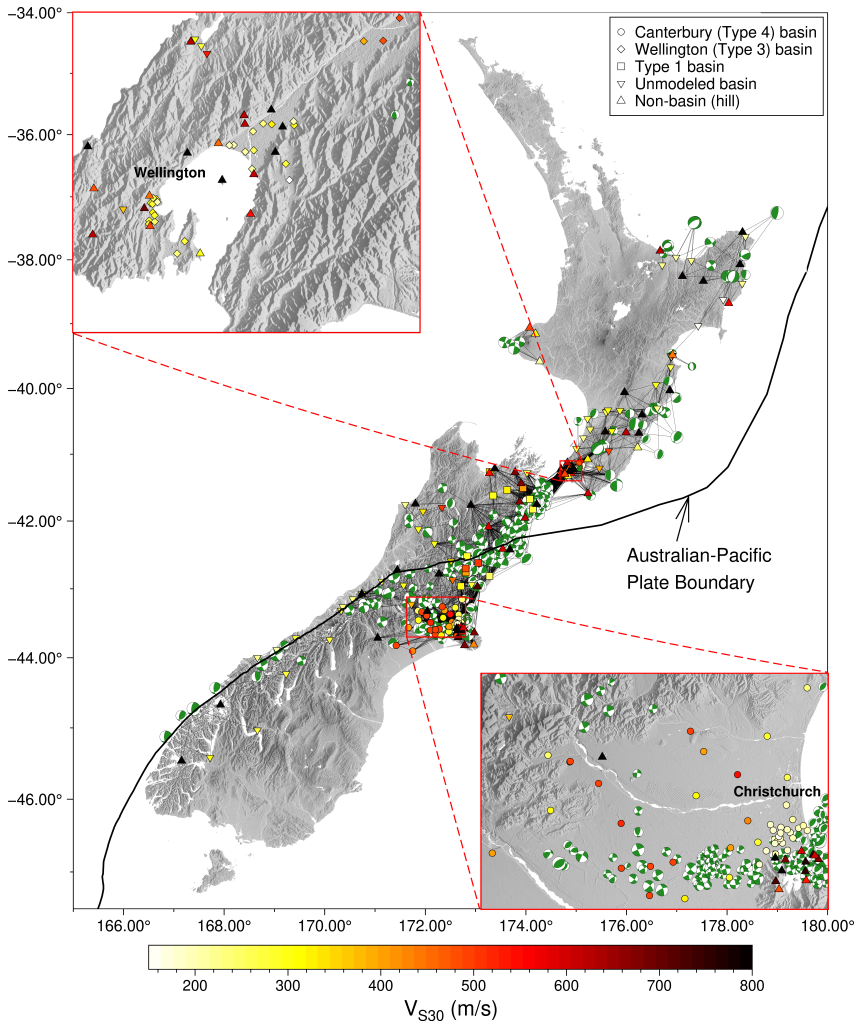

Figure 1. Spatial distribution of the 212 stations and 479 earthquake sources considered across New Zealand. Stations are represented with different symbols according to their basin type category and are color-coded by V_{S30}. Earthquake sources are shown as green-and-white focal mechanism symbols ("beach balls"), with the symbol size scaled proportionally to the earthquake magnitude. Schematic ray paths corresponding to the 5218 ground motions considered are shown as black lines connecting sources and stations.

multiple datasets, including seismic reflection lines, petroleum and water-well logs, cone penetration tests, and geologic maps. Wellington is classified as a Type 3 subregion, where borehole, standard penetration test, horizontal-to-vertical spectral ratio, and V_S

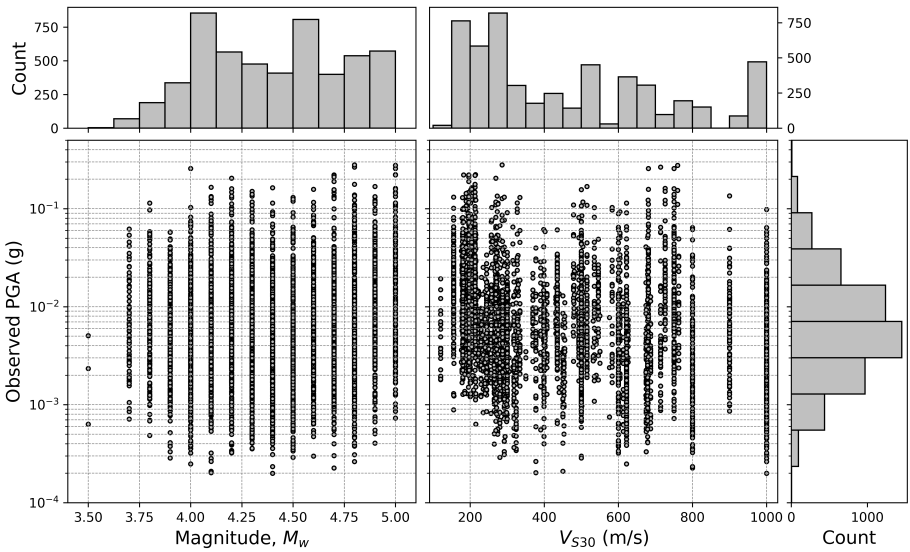

Figure 2. Ground motion distribution in terms of observed PGA versus magnitude and V_{S30}. The observed PGA is computed as the geometric mean of the two horizontal components. Magnitudes for the 479 events considered are rounded to one decimal place.

data were considered (Semmens et al. 2010; Boon et al. 2010). The remaining subregions are classified as Type 1. For locations outside these subregions, the V_{S30}-based Ely et al. (2010) geotechnical layer model, along with the Foster et al. (2019) V_{S30} map (based on geology, topographic slope, and V_S data), is used to constrain the near-surface velocity.

In order to synthesize trends in simulation prediction residuals, Tiwari et al. (2024) classified the sites in Lee et al. (2022) into four geomorphic categories based on Nweke et al. (2022): "Basin", "Basin-edge", "Valley", and "Hill" sites. By combining the subregion classification of the NZVM v2.02 and the identified hill sites, a basin-type categorization has been considered (Tiwari et al. 2024, ongoing work), which includes five categories: "Canterbury (Type 4) basin", "Wellington (Type 3) basin", "Type 1 basin", "Unmodeled basin", and "Non-basin" (hill) sites. In this classification, "Unmodeled basin" sites correspond to non-hill locations outside the subregions with explicit basin modeling in the NZVM v.2.02, and represent sites modeled by the V_{S30}-based geotechnical layer. Figure 1 illustrates the basin-type category assigned to each site, which is subsequently used in this study along with the geomorphic categories to interrogate the validation results.

Site properties

Figure 3 presents the distribution of V_{S30}, $Z_{1.0}$, and T_0 (fundamental site period) for all stations considered, disaggregated by basin type category. These site parameters were determined by Wotherspoon et al. (2024) from direct measurements or inferred based on other sources; except for the D09C and WSTS sites, for which values from Lee et al. (2022) were considered. Wotherspoon et al. (2024) also assigned a quality rating (Q1, Q2, or Q3) to indicate how well each parameter is constrained by data. For V_{S30}, Q1 indicates the use of robust site-specific V_S measurements within a few tens of meters of the station; Q2 implies that V_S measurements shallower than 30 m were used; and Q3 means that no site-specific data was available, in which case the national V_{S30} models by Foster et al. (2019) and Perrin et al. (2015) were considered. In this study, 20.8% of the sites considered have V_{S30} rated as Q1, 4.7% as Q2, and 74.5% as Q3. For $Z_{1.0}$, only 2.8% of the sites are classified as Q1 (i.e., they have well-constrained values based on measurements), while for T_0, this proportion corresponds to 67.9%.

Figure 3 illustrates that most of the $V_{S30} \leq 200$ m/s values are in the Canterbury basin (concentrated in the Christchurch metropolitan area, as shown in Figure 1), and most of the $V_{S30} \geq 550$ m/s values correspond to hill sites. The figure also displays the V_{S30}-$Z_{1.0}$ correlation used in Bayless and Abrahamson (2019) (based on Chiou and Youngs (2014), for California and non-Japan regions) along with additional lines representing a factor of five above and below this correlation model (i.e., the model multiplied and divided by five, respectively), to identify sites that are significantly deeper or shallower than an 'average site' conditioned on V_{S30}. Most of the sites in the Canterbury basin are seen to lie close to or above the Bayless and Abrahamson (2019) correlation, which is explained by the particularly deep basement rock in this region (Lee et al. 2017), and also reflected in the high T_0 values for this basin. In contrast, most of the Wellington sites fall below the Bayless and Abrahamson (2019) correlation, with a significant number of sites even below the lower factor-of-five boundary, indicating a particularly shallow basin (e.g., Hill et al. 2022). A similar distribution is observed for Type 1 and unmodeled basin sites.

Methodology

Ground-motion simulation method

The ground-motion simulations used in this study were conducted by Lee et al. (2022) using the hybrid broadband method of Graves and Pitarka (2010, 2015, 2016) (herein

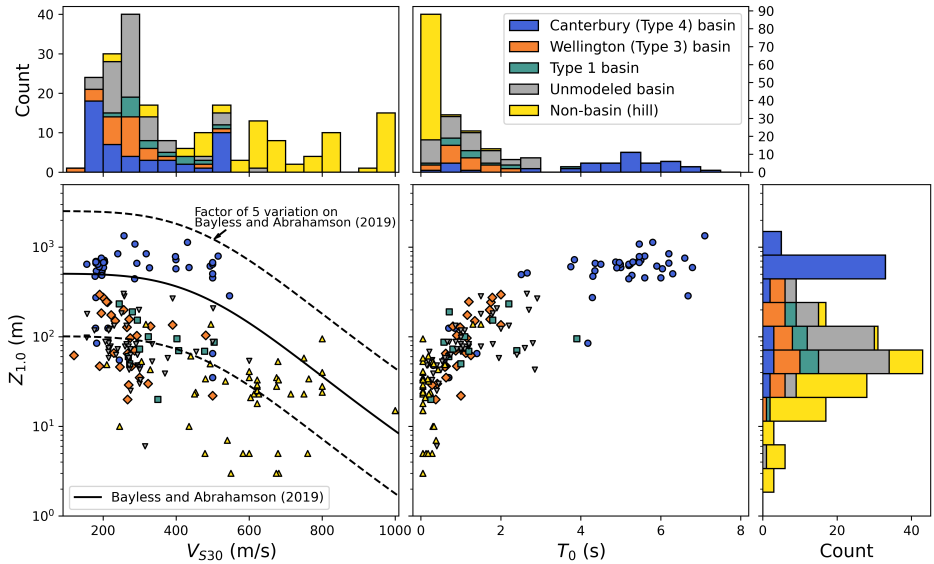

Figure 3. V_{S30}, $Z_{1.0}$, and T_0 distributions for the sites considered, disaggregated by basin type category. The V_{S30} vs $Z_{1.0}$ plot includes the Bayless and Abrahamson (2019) $V_{S30} - Z_{1.0}$ correlation, and boundaries with a factor of five above and below this correlation. The maximum V_{S30} value represented in the x-axis of the left panels is 1010 m/s, but there are three sites with a higher value: DCZ, INZ, and MSZ, with $V_{S30} = 1500$ m/s. The site parameters for the stations D09C and WSTS were not provided by Wotherspoon et al. (2024). The V_{S30} values considered for these two stations are those reported by Lee et al. (2022), and the corresponding $Z_{1.0}$ values were estimated based on the NZVM v2.02 (T_0 is not provided for these two sites).

referred to as the GP method for brevity). In the GP method, a comprehensive 3D physics-based approach is utilized for the low-frequency (LF) simulation component, and a simplified physics-based approach is used for the high-frequency (HF) simulation component. The LF simulation is based on a kinematic representation of the earthquake fault rupture and explicit 3D viscoelastic wave propagation. The HF simulation relies on a stochastic representation of source radiation and a Green's function based on a 1D V_S structure. After being adjusted for site effects (as described below), the LF and HF simulated waveforms are combined using a matched filter to produce a broadband (BB) ground motion. A LF-HF transition frequency of $f = 1$ Hz was adopted based on the evidence that ground motion can be effectively represented as a stochastic time series at frequencies above 1.0 Hz (e.g., Hanks and McGuire 1981). For the LF simulation, the NZVM (Thomson et al. 2020) v2.02 was used, with a finite difference grid spacing of 100 m and a minimum V_S of 500 m/s. Given the use of a fourth-order spatial finite

difference scheme, this configuration supports proper seismic wave propagation up to 1 Hz (e.g., Baker et al. 2021; Graves and Pitarka 2010). For the HF simulation, a generic V_S profile (Lee et al. 2022) representative of a basin site, with a minimum V_S of 500 m/s at the top, and a constant high-frequency attenuation parameter $\kappa_0 = 0.045$ s were used for the whole country.

V_{S30}-based site correction factors

Given some of the limitations of the LF and HF simulation approaches, such as the relatively coarse spatial resolution (e.g., grid spacing of 100 m for the LF simulation) and high minimum V_S (e.g., 500 m/s in this study) considered, a posterior site adjustment must be applied to account for unmodeled site effects (Kuncar et al. 2025a). In this study, this adjustment is performed using a V_{S30}-based site factor (SF) applied in the frequency domain, which is determined using Methods 1 and 2 examined in Kuncar et al. (2025a). Method 1 has been adopted in several previous studies (e.g., Graves and Pitarka 2010; Lee et al. 2022) and is used throughout most of this paper, while Method 2 is explored in the "Incorporating a host-to-target V_S-profile adjustment" section.

Figure 4 illustrates the SF application workflow. The simulated acceleration time series (a_{sim}) generated by the LF and HF simulation approaches are first converted to the frequency domain. Separate SFs (SF_{LF} and SF_{HF}) are then applied to the FAS of the LF and HF components, respectively. The modified (LF and HF) FAS are subsequently converted back to the time domain and merged to produce an adjusted BB acceleration time series (a_{adj}). In previous studies either both SF_{LF} and SF_{HF} have been considered (e.g., Graves and Pitarka 2010; Lee et al. 2020), or only SF_{HF} has been applied (e.g., Lee et al. 2022). Herein, these two approaches are referred to as "LF+HF" and "HF only", respectively. This aspect is investigated in the "Frequency range of SF application" section.

The V_{S30}-based SF (SF_1, corresponding to Method 1 in Kuncar et al. 2025a) is derived using a semi-empirical GMM (e.g., Bayless and Abrahamson 2019). GMMs generally predict the mean value of a given intensity measure (IM) in natural log scale, conditioned on a specific earthquake rupture and site, as

$$\mu_{\ln IM}(rupture, site) = f_E + f_P + f_S \quad (1)$$

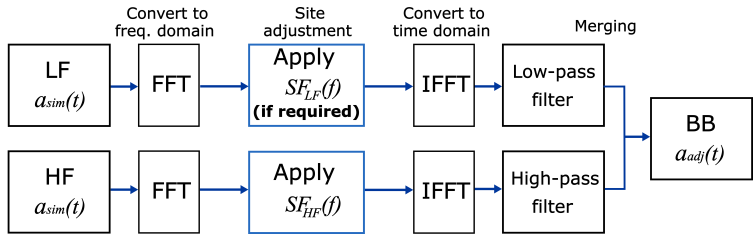

Figure 4. SF application workflow. FFT and IFFT are the fast Fourier transform and inverse fast Fourier transform algorithms, respectively. In principle, SF_{LF} should not be applied, but in practice it may be required to capture site effects not properly modeled in the LF simulation component.

where f_E, f_P, and f_S are source, path, and site response scaling factors, respectively. The site response scaling factor (f_S) can be generally expressed as the sum of three terms (e.g., Campbell and Bozorgnia 2014; Bayless and Abrahamson 2019):

$$f_S = f_L + f_{NL} + f_{sed} \tag{2}$$

where f_L and f_{NL} represent the scaling of the linear and nonlinear site response with V_{S30}. Additionally, the term f_{NL} is a function of a given IM at a reference condition (e.g., peak ground acceleration at a rock or stiff soil site condition). The term f_{sed} usually accounts for the difference between the site-specific $Z_{1.0}$ (depth to $V_S = 1.0$ km/s) and the expected $Z_{1.0}$ conditioned on V_{S30} (e.g., Bayless and Abrahamson 2019). Therefore, f_{sed} requires a site-specific estimate of $Z_{1.0}$ in addition to V_{S30}. The incorporation of f_{sed} into the SF is investigated in the "Sediment depth consideration" section.

Based on the above expressions, SF_1 is computed as the ratio between $\exp(f_S)$ for the "actual" (i.e., site-specific; $f_{S,actual}$) and "simulation" ($f_{S,sim}$) conditions (the source and path scaling factors are common to both and therefore cancel out), as

$$SF_1(f) = \frac{\exp[f_{S,actual}(f)]}{\exp[f_{S,sim}(f)]} = \frac{\exp(f_{L,actual} + f_{NL,actual})}{\exp(f_{L,sim})} \tag{3}$$

where the f_{NL} is not included in the denominator for consistency with the simulation method adopted, which does not directly include soil nonlinearity. $f_{L,actual}$ and $f_{NL,actual}$ depend on the site-specific V_{S30} value, and $f_{L,sim}$ depends on the V_{S30} value implicit in the simulation (e.g., 500 m/s for the HF simulation in this study).

Given the SF application workflow presented in Figure 4, it is evident that the semi-empirical GMM used should, in principle, be formulated for FAS. However, GMMs for

FAS (or EAS) have only recently been developed (e.g., Bora et al. 2019; Bayless and Abrahamson 2019; Shi 2019; Campbell and Bozorgnia 2025). For this reason, several previous studies (e.g., Graves and Pitarka 2010; Pitarka et al. 2020; Lee et al. 2022; Graves 2022) have utilized GMMs formulated for SA (e.g., Campbell and Bozorgnia 2014; Boore et al. 2014) to approximately compute SF_1 instead. In particular, previous nationwide validation efforts in NZ (Lee et al. 2022; Dupuis et al. 2025) have only considered the CB14 model (Campbell and Bozorgnia 2014) developed for SA. In this study, four alternative GMMs are considered to determine SF (i.e., $f_{L,actual}$, $f_{NL,actual}$, and $f_{L,sim}$): two GMMs for the average horizontal component of SA and two GMMs for EAS. The SA-based GMMs are the CB14 (Campbell and Bozorgnia 2014) and the BSSA14 (Boore et al. 2014) models, and the EAS-based GMMs are the BA18 (Bayless and Abrahamson 2019) and the CB24 (Campbell and Bozorgnia 2025) models. All these models were derived using the Next Generation Attenuation-West2 database (Ancheta et al. 2014), containing data from different countries, but primarily from California. In addition, the nonlinear site-response scaling factors were constrained by parametric models derived from multiple 1D equivalent-linear or nonlinear site-response analyses (Walling et al. 2008; Kamai et al. 2014; Hashash et al. 2018). For the CB14 and CB24 models, only the shallow site response term, without the adjustment for Japan, is considered. In the case of the CB24 model, Model ES (i.e., the recommended version of the model) is used. It is important to note that, unlike the BA18 and BSSA14 models, the CB14 and CB24 site scaling factors are unconstrained at large V_{S30}. This can be problematic when very large V_{S30} values are considered (see Electronic Supplement B).

It should be noted that although several GMMs have been developed for New Zealand, their site response components (i.e., f_S) have been adopted from California-based models similar to those used in this study. For example, the ground-motion characterization model for the 2022 NZ National Seismic Hazard Model (Bradley et al. 2024) included three NZ-specific GMMs for SA: the B13 (Bradley 2013), A22 (Atkinson 2022, 2024), and S22 (Stafford 2022) models. These GMMs adopted f_S from the California-based Chiou and Youngs (2008), Seyhan and Stewart (2014), and Chiou and Youngs (2014) models, respectively.

Figure 5 illustrates the different SFs for the example sites RHSC ($V_{S30} = 286$ m/s) and CBGS ($V_{S30} = 197$ m/s), located in Christchurch, for an input HF PGA of 0.01 g, which is representative of the amplitudes from the small-magnitude earthquakes considered. Figures 5a and 5b present the site factors (for the RHSC and CBGS sites, respectively) as computed using Equation 3 (for the SA-based CB14 and BSSA14

models, the frequencies were obtained by taking the inverse of the oscillator periods). Figures 5c and 5d show the corresponding site factors that are actually used for the site adjustment, which contain low- and high-frequency truncations recommended in the literature. As observed in Figures 5a and 5b, the EAS-based models (BA18 and CB24) incorporate high-frequency attenuation, which is consistent with theory (e.g., Baker et al. 2021, Ch.5), while the SA-based models (CB14 and BSSA14) do not include this feature due to the difference in scaling between SA and FAS (e.g., Bora et al. 2016). As shown in Figures 5c and 5d, the SA-based SFs (CB14 and BSSA14) were truncated to $SF = 1$ for frequencies $f \geq 15$ Hz, with a taper from $f = 10 - 15$ Hz, to mitigate major inconsistencies with their application in the FAS domain (e.g., following de la Torre et al. 2020; Razafindrakoto et al. 2021; Lee et al. 2022). In addition, all site factors are truncated to $SF = 1$ for frequencies $f \leq 0.2$ Hz, with a taper from $f = 0.2 - 0.5$ Hz, to avoid double-counting deep 3D velocity structure effects already captured by the LF simulation (e.g., following Lee et al. 2020; de la Torre et al. 2020). A similar low-frequency taper was also considered by Graves and Pitarka (2010) and Matinrad and Petrone (2025) for the same reasons.

Prediction residual partitioning

Residual analysis is conducted to assess simulation performance with alternative site factors, considering the entire ground-motion database. For a given intensity measure (IM), the prediction residual (Δ_{es}) for the event e recorded at the site s is defined as

$$\Delta_{es} = \ln(IM_{obs})_{es} - \ln(IM_{sim})_{es} \tag{4}$$

where $\ln(IM_{obs})_{es}$ is the natural logarithm of the observed IM and $\ln(IM_{sim})_{es}$ is the natural logarithm of the simulated IM. Δ_{es} can be partitioned into different components of ground motion variability (Atik et al. 2010) via a crossed linear mixed-effects regression algorithm (Stafford 2014; Bates et al. 2015), as follows:

$$\Delta_{es} = a + \delta S2S_s + \delta B_e + \delta W_{es}^0 \tag{5}$$

where a is the (global) model prediction bias, representing the residual fixed effect across all sites and events; $\delta S2S_s$ is the systematic site-to-site residual for the site s; δB_e is the systematic between-event residual for the event e; and δW_{es}^0 is the "remaining" within-event residual for the event e recorded at the site s, which includes factors that are not systematically captured by a, $\delta S2S_s$, and δB_e. Assuming that $\delta S2S_s$, δB_e, and δW_{es}^0 are

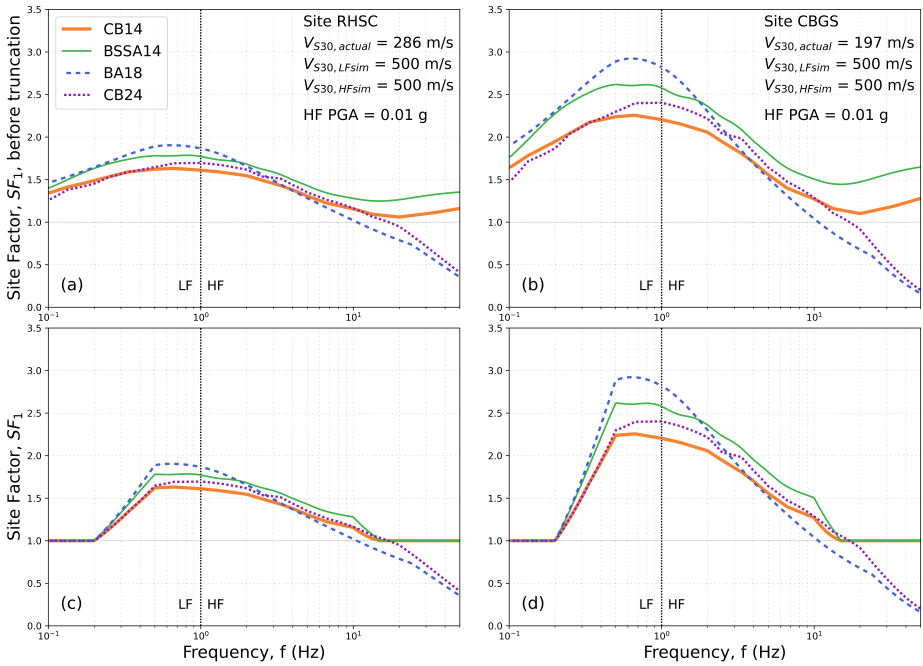

Figure 5. Site factors derived using alternative GMMs for the RHSC and CBGS sites. (a) and (b) illustrate the site factors without any truncation for RHSC and CBGS, respectively. (c) and (d) show the corresponding site factors after applying low- and high-frequency truncations. CB14 and BSSA14 are SA-based models, whereas BA18 and CB24 are EAS-based models.

independent and normally distributed random variables, with zero mean and variances of ϕ^2_{S2S}, τ^2, and ϕ^2_{ss}, respectively, the total variance (σ^2) can be expressed as

$$\sigma^2 = \phi^2_{S2S} + \tau^2 + \phi^2_{SS} \tag{6}$$

The sum $(a + \delta S2S_s)$ is herein referred to as the "systematic residual" and represents the systematic portion of the residual at a given site s. The IMs considered are: 5%-damped pseudo-spectral acceleration (SA) at vibration periods between 0.01 and 10 s; Fourier amplitude spectrum (FAS) at frequencies between 0.1 and 20 Hz; peak ground acceleration (PGA); peak ground velocity (PGV); cumulative absolute velocity (CAV); Arias intensity (AI); and $5\% - 75\%$ and $5\% - 95\%$ significant duration (D_{s575} and D_{s579}, respectively). FAS is smoothed using Konno-Ohmachi matrices with bandwidth parameter $b = 40$, a value typically considered (e.g., Bora et al. 2019; Baker et al. 2021) to preserve the frequency resolution while avoiding over-smoothing. All these IMs are

computed from the two horizontal components. In the case of FAS, the two components are combined using the EAS definition (e.g., Bayless and Abrahamson 2019). For the other IMs, the two components are combined using the geometric mean.

Results

Effect of alternative site-response models

Figure 6 shows the model bias, a, and site-to-site standard deviation, ϕ_{S2S}, for all GMMs and IMs considered. The results are shown for both the "HF only" and "LF+HF" application approaches. Figure 6 also presents the results for the simulation without site adjustment ("no site adjustment"), which is generated by merging the LF and HF simulated waveforms without applying any site factor. Figures 6a and 6c show that the "no site adjustment" simulation systematically underpredicts the ground motions for SA($T < 0.3$ s), SA($T > 0.8$ s), EAS($f < 1.8$ Hz), and all the remaining IMs considered. Significant overprediction is observed for EAS($f > 2.5$ Hz) before applying the SF, suggesting inaccuracies in the modeling of source, path, and global site attenuation effects in the HF simulation. The application of the (HF only) SFs generally reduces the underprediction for PGA, PGV, CAV, and SA at very short and very long periods, but generates overprediction for AI and SA in the intermediate period range (approximately $0.1 < T < 1$ s). For EAS, underprediction is only reduced within a narrow frequency band (approximately $0.7 < f < 1$ Hz), corresponding to the LF range influenced by the HF SF due to the high-pass filter considered when merging the LF and HF components (Graves and Pitarka 2010); and an increase in the overprediction is generally exhibited at higher frequencies. At very high frequencies (e.g., $f > 10$ Hz) the EAS-based BA18 model, which accounts for high-frequency attenuation, allows for a reduction in the overprediction. For all GMMs, the incorporation of the SF_{LF} ("LF+HF" application approach) produces significant overprediction for SA at long vibration periods ($T > 1$ s) and EAS at low frequencies ($f < 1$ Hz).

Figure 6b and 6d indicate that for the "no site adjustment" simulation, the highest values of site-to-site variability are produced for SA($0.4 < T < 1.5$ s), AI, EAS($0.8 < f < 2$ Hz), and particularly for EAS($f > 10$ Hz). Due to the differences between SA and FAS (Bora et al. 2016; Stafford et al. 2017), this significant variability at very high frequencies does not manifest for SA at short periods in an active tectonic region such as NZ. The application of the alternative SFs reduces the site-to-site variability for several IMs. In the case of SA, this reduction is particularly strong at $0.3 < T < 1.5$ s, and

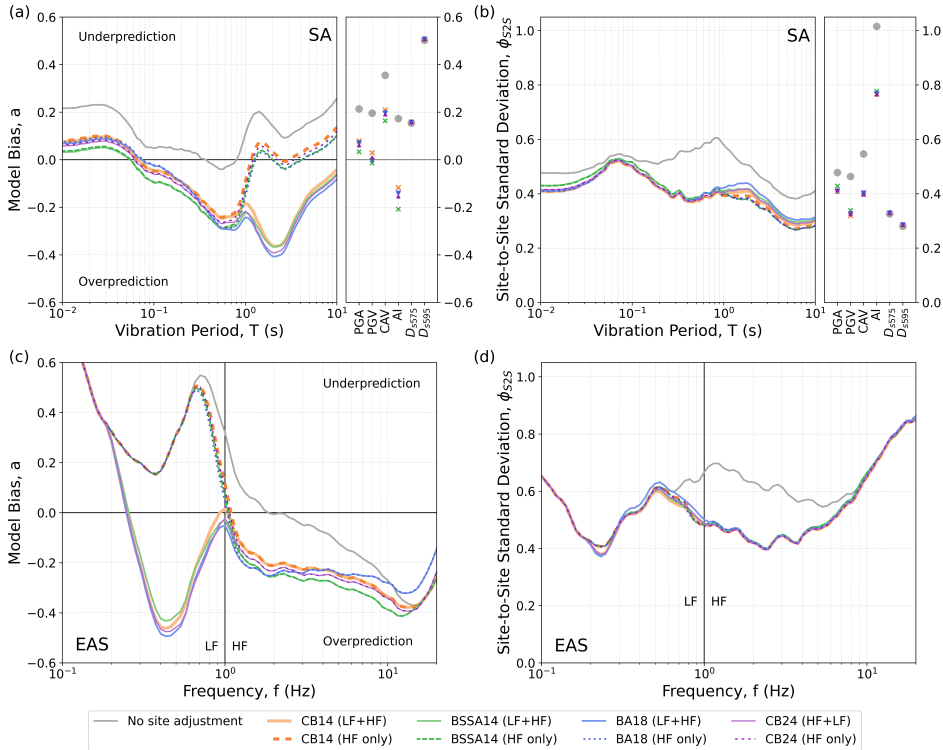

Figure 6. Model prediction bias, a, and site-to-site standard deviation, ϕ_{S2S}, for alternative ground-motion models and application frequency ranges: (a) a and (b) ϕ_{S2S} for SA, PGA, PGV, CAV, AI, D_{s575}, and D_{s595}. (c) a and (d) ϕ_{S2S} for EAS. Results for PGA, PGV, CAV, AI, D_{s575}, and D_{s595} are only presented for the HF application case (similar bias and variability are obtained for the LF+HF application for these IMs).

for EAS at $0.9 < f < 4.0$ Hz. However, at $f > 10$ Hz no reduction is obtained. This increasingly high site-to-site variability displayed at very high frequencies is consistent with previous observations across different regions and site-response models (Pilz et al. 2025). The significant duration IMs are not modified by the SFs considered, which is observed in both the site-to-site variability and model bias plots.

The SA-based CB14 model was adopted in several previous validation studies in NZ (e.g., Bradley et al. 2017b; Razafindrakoto et al. 2018; de la Torre et al. 2020; Lee et al. 2020, 2022). Figure 6 shows that more recently developed EAS-based GMMs, such as BA18 and CB24, exhibit a similar performance in terms of model bias and site-to-site variability, at least for small-magnitude events. Considering that the SF is applied in the Fourier spectral domain, this suggests that, for consistency, FAS- or EAS-based GMMs

(such as those considered in this article) should be adopted in future studies. In addition to the reduction of EAS model bias at very high frequencies, illustrated in Figure 6c for the BA18 model, the use of EAS-based models avoids the need for artificial truncation of the SF at high frequencies. It can also facilitate the use of site-specific κ_0 values (e.g., Van Houtte et al. 2018) for the HF simulation in future studies. The selection of κ_0 in the HF simulation needs to take into account the additional HF attenuation incorporated by the SF to avoid double-counting high-frequency attenuation, and the use of a EAS-based model allows for a more transparent determination of this extra attenuation implicit in the SF. In the context of simulation-based PSHA, alternative GMM-based SFs could be considered within a site response logic tree (Rodriguez-Marek et al. 2021), and the results shown in Figure 6 could help to inform the relative weights assigned to different models.

Relationship between EAS and SA residuals

Figure 6 illustrated significant differences between the EAS and SA residuals. While EAS is a direct representation of the ground motion, SA reflects the response of a single-degree-of-freedom system to this input ground motion, which, at a given vibration period, is influenced by FAS at a range of frequencies (Bora et al. 2016; Stafford et al. 2017). A perfectly accurate ground-motion prediction would result in zero systematic residual for both IMs. Previous validation studies in NZ (e.g., Razafindrakoto et al. 2018; de la Torre et al. 2020; Lee et al. 2020, 2022) have focused on SA due to its relevance in engineering applications, but a more direct assessment of ground-motion simulations should consider EAS, which avoids the inter-frequency contamination produced in the SA domain. The use of EAS also allows for the separate evaluation of the LF and HF simulation approaches.

To further understand the relationship between EAS and SA, Figure 7 superimposes the EAS and SA mean systematic residuals, $a + \delta S2S_{s,mean}$ (in addition, Supplemental Figures A.1 and A.2 in Electronic Supplement A include the 95% confidence interval of the mean systematic residual, for EAS and SA, respectively). Two cases are considered: "no site adjustment" and simulation adjusted using the (HF only) SF computed with the EAS-based BA18 model. The SA residuals are plotted as a function of the (oscillator) vibration period, T, whereas the EAS residuals are plotted as a function of the (signal) FAS period, $1/f$. Herein, the word "period" will be used indistinctly for both IMs, although strictly speaking it has a different meaning in each case. Figure 7a, which incorporates all sites (i.e, the mean systematic residual corresponds to a), shows that before applying the SF, the systematic underprediction at long periods is stronger for

EAS than for SA. Since the SF is only applied to the HF simulation component, then the application of the SF yields no reduction in the model bias for EAS at periods longer than $\approx$ 1.5 s (in the period range $\approx$ 1.0-1.5 s there is an influence from the HF simulation due to the high-pass filter applied when merging both components, illustrated in Figure 4). However, bias is reduced to almost zero for SA within the equivalent period range. This suggests that long-period SA are influenced by shorter FAS periods, resulting in a reduction in the long-period SA residuals. Stafford et al. (2017) showed that for small-magnitude events (as considered in this study), which have a relatively high corner frequency, long-period SA site response is influenced by a broad range of FAS frequencies, but this effect diminishes as magnitude increases. At short periods, the simulation without adjustment displays increasing levels of overprediction for EAS toward shorter periods. However, this is not manifested for SA at the equivalent period range because short-period SA are controlled by a broader FAS period range. The EAS systematic overprediction at very short periods, observed in both the no-adjustment and BA18-based adjustment cases, suggests that using a generic $\kappa_0 = 0.045$ s value in the HF simulation may not be appropriate. Considering that κ_0 is often correlated with V_{S30} (e.g., Bayless and Abrahamson 2019), Supplemental Figure A.3 investigates the dependence of EAS residuals at very short periods with V_{S30}, but without identifying any significant trend.

The systematic underprediction observed at EAS periods longer than 1.5 s in Figure 7a (which cannot be corrected by applying an HF site factor) suggests that there are deficiencies in the velocity model used in the LF simulation and/or limitations in its implementation in the finite-difference computation. Figures 7b-f indicate that this underprediction is not equally strong for all basin-type categories. The Canterbury (Type 4) basin (i.e., the basin model better constrained by data in the NZVM v2.02) and non-basin sites exhibit the lowest EAS systematic residual at long periods, whereas unmodeled basin and Wellington (Type 3) basin sites display the strongest underprediction. Although the Wellington basin has a relatively good characterization in the NZVM v2.02, this corresponds to a shallow basin, as inferred from Figure 3 and from the available basin models in that region (Semmens et al. 2010; Hill et al. 2022). As discussed in Kuncar et al. (2025b), this means that the 100-m spatial discretization considered in the LF simulation is insufficient to properly represent the sediment-rock interface and capture resonance and basin-edge effects. Systematic analysis of ground-motion residuals from semi-empirical GMMs (e.g., de la Torre et al. 2024) has shown that soft sedimentary basin sites in Wellington strongly amplify SA in the 0.5-2.0 s period

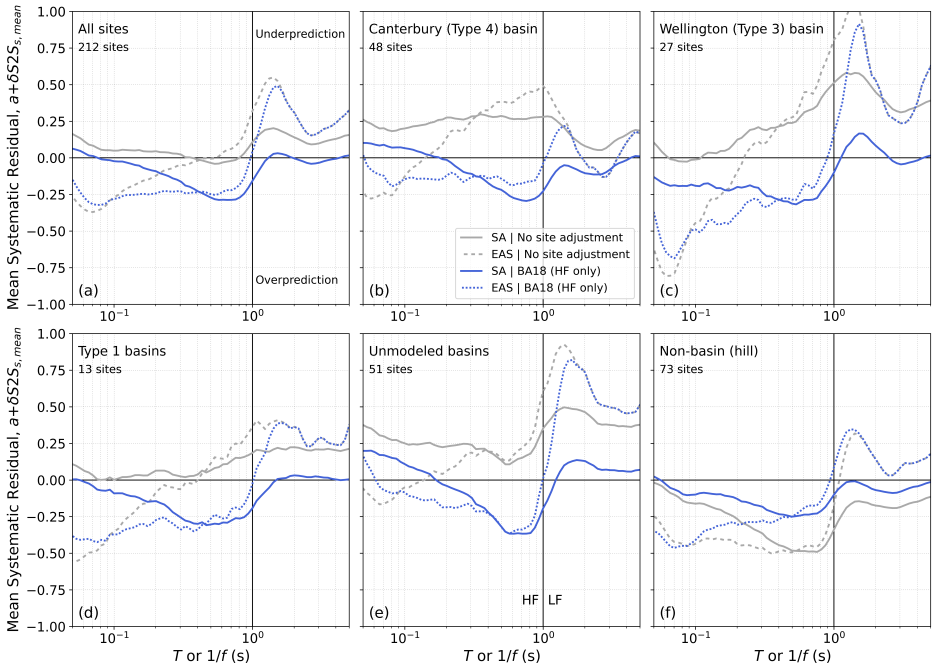

Figure 7. Mean systematic residual, $a + \delta S2S_{s,mean}$, for EAS and SA, for the simulation with no site adjustment and for the (HF only) BA18 model. The mean systematic residuals are plotted for (a) all sites, and for (b) Canterbury (Type 4) basin, (c) Wellington (Type 3), (d) Type 1 basin, (e) unmodeled basin, and (f) non-basin (hill) sites.

range. Also, the presence of basin-edge effects (Kawase 1996) in this basin has been inferred from observations and numerical models (e.g., Bradley et al. 2018; McGann et al. 2021).

These observations demonstrate the strong impact of good-quality basin modelling on long-period EAS prediction performance. Figure 7 illustrates that the corresponding impact on long-period SA is weaker (i.e., the SA residuals are less sensitive to basin type and are generally centered around zero at long periods). However, due to the scenario-dependent FAS frequency-range contribution to long-period SA, this impact can increase for larger-magnitude events or if modifications are performed to the HF simulation (e.g., such that the HF overprediction is reduced). This illustrates one of the advantages of considering EAS residuals (versus SA residuals alone) to evaluate the performance of the LF simulation component.

Regarding the short-period EAS, Figures 7b-f show that the level of EAS overprediction is also dependent on the basin-type category, although in this case this dependence reflects regional differences in the accuracy of the HF simulations and the BA18-based SF. The strongest overprediction is observed for the Wellington (Type 3) basin, Type 1 basin, and non-basin (hill) sites. Kuncar et al. (2025b) found that stiff soil and rock sites in Wellington also display this systematic overprediction at short periods, suggesting that the overprediction observed for basin sites is mainly caused by inaccuracies in the modeling of source and path effects in this region. The incorporation of additional high-frequency attenuation through the BA18 model reduces the systematic overprediction for all basin categories at periods shorter than 0.09 s relative to the "no site adjustment" case.

This section demonstrates that the use of EAS systematic residuals enables a more direct and transparent assessment of the LF and HF simulation performance, compared to SA systematic residuals used in previous studies. The analysis of EAS systematic residuals revealed systematic differences across basin-type categories (differences that are masked when using SA). In particular, prediction performance at long EAS periods was shown to be strongly influenced by basin type.

Frequency range of SF application

While SF_{HF} is generally required to capture shallow site effects (which mainly affect $f > 1$ Hz), it is not yet clear to what extent SF_{LF} is needed when a 3D velocity model that explicitly incorporates sedimentary basins is used in the LF simulation and a LF-HF transition frequency of 1 Hz is adopted. For example, Lee et al. (2022) only considered SF_{HF} (i.e., $SF_{LF} = 1$), and showed that this reduces the systematic long-period SA overamplification previously observed in Lee et al. (2020), where both SF_{LF} and SF_{HF} were applied. This is also observed in Figure 6a for all GMMs. However, as inferred from the discussion in the "Relationship between EAS and SA residuals" section, part of the systematic overamplification obtained at long-period SA when the SF is applied to both the LF and HF components can be explained by the influence of FAS over a broad range of frequencies, rather than being a direct feature of the LF simulation. When SF is only applied to the HF simulation (as in Lee et al. 2022), the net effect is a near-zero bias at long-period SA, but EAS residuals display systematic underprediction over the equivalent period range (e.g., Figure 7a). This suggests that including some level of LF site amplification (i.e., $SF_{LF} \geq 1$) is needed to improve LF simulation performance (i.e., LF EAS predictions) in a significant number of sites (Canterbury being an exception).

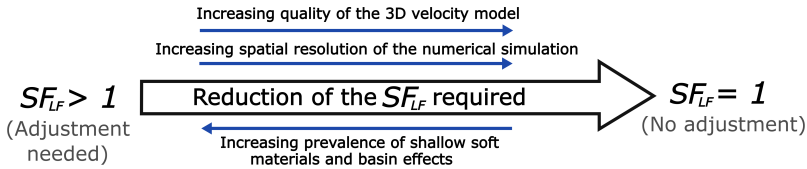

Figure 8. Conceptual illustration of the factors contributing to the need for a LF site adjustment (SF_{LF}).

As illustrated conceptually in Figure 8, the magnitude of the SF_{LF} will depend on several factors, which are related to both the quality of the LF simulation and the specific site conditions. If the 3D velocity model used is well characterized (e.g., based on a large amount of geophysical and geotechnical data) and the grid spacing considered in the finite-difference computation is fine enough to capture the main features controlling low-frequency site response (e.g., deep impedance contrasts, basin geometry), a less significant (or no) LF adjustment will be required. All other things being equal, if basin effects are particularly strong in a given region, a higher LF site adjustment is more likely to be needed due to the difficulties in capturing these complex effects solely based on the LF physics-based simulation approach of the GP method. Even in the case where the underlying 3D velocity model is completely accurate, if its implementation in the LF simulation considers a relatively coarse spatial discretization (e.g., a grid spacing of 100 m and a minimum V_S of 500 m/s, as considered in this study), the LF simulation will not properly model the influence of the surficial materials on the LF ground motion. This is particularly relevant in the case of relatively soft soil deposits, which may have a shallow site response (e.g., impedance and resonance effects caused by the soils in the $\approx$ top 100 m) that influences the LF range (as observed in Kuncar et al. 2025b).

Given that all factors described in Figure 8 coexist, and their relative characteristics and influence vary region-to-region and location-to-location within a given region, it is not possible to specify *a priori* the optimal SF_{LF} required. However, validation against observations can inform proper application protocols for this site factor in forward applications. As previously shown in Figure 7, "Unmodeled" and "Wellington (Type 3) basin" sites display, on average, the more significant underprediction for EAS in the LF range when only SF_{HF} is applied. However, the level of LF underprediction is not equally strong for all sites in a given category. Figure 9 displays the distribution of site average LF systematic residuals across NZ, for the "HF only" SF application case, using the BA18 model. This average residual was computed as the systematic residual for EAS averaged over the frequency range $0.3 - 1.0$ Hz. While most of the sites in the

"Unmodeled basin" or "Wellington (Type 3) basin" categories display positive residuals (i.e., underprediction), there are some sites in these categories presenting a near-zero systematic residual or overprediction. Also, it can be observed that several sites in other basin-type categories display LF underprediction. This is the case for "Canterbury (Type 4) basin" sites at the west of the Canterbury basin (shown in the bottom-right inset). Even though the Canterbury basin is, in general, well characterized in the NZVM v2.02, it is possible that this sub-region contains deficiencies in the velocity model. Also, the location of these sites near the edge of the basin suggests that they may be affected by basin-edge effects not captured in the LF simulation due to the spatial discretization considered. In contrast, systematic overprediction (negative bias) is observed for sites located further east, but still west of Christchurch. Based on measured deep V_S profiles (Deschenes et al. 2018), Kuncar et al. (2025b) showed that in this area, the actual V_S in the top 100-700 m is significantly higher than that represented in the NZVM v2.02. This discrepancy can explain the observed low-frequency overamplification (as the simulation assumes softer conditions than those present in reality) and indicates that the NZVM needs to be updated in this area by integrating the site-characterization data from Deschenes et al. (2018) and other sources.

To further examine the need for additional LF amplification across all sites considered, and to help establish an application protocol for SF_{LF}, Figure 10 presents the distribution of sites for which the application of the LF site factor is considered beneficial across different categories. This is assessed using the following expression:

$$\Delta R = |R_{HF}| - |R_{LF,HF}| \tag{7}$$

where R_{HF} is the LF systematic residual (EAS systematic residual averaged over $0.3 - 1.0$ Hz) when only SF_{HF} is applied ("HF only" SF application approach), and $R_{LF,HF}$ is the corresponding residual for the case where both SF_{LF} and SF_{HF} are applied ("LF+HF" SF application approach). If ΔR is positive, it means that the "LF+HF" approach reduces the absolute value of the LF systematic residual relative to the "HF only" approach. Based on the examination of the ΔR results, three cases were identified for the SF_{LF} application: (1) $\Delta R \leq 0$: increase of residual; (2) $0 < \Delta R < 0.1$: slight residual reduction; and (3) $\Delta R \geq 0.1$: considerable residual reduction (representing a significant benefit obtained by the application of SF_{LF}). Figure 10a shows that the "'Wellington (Type 3) basin" category has the highest proportion of sites with a considerable reduction in the LF systematic residuals, followed by "Unmodeled basin", and "Type 1 basin".

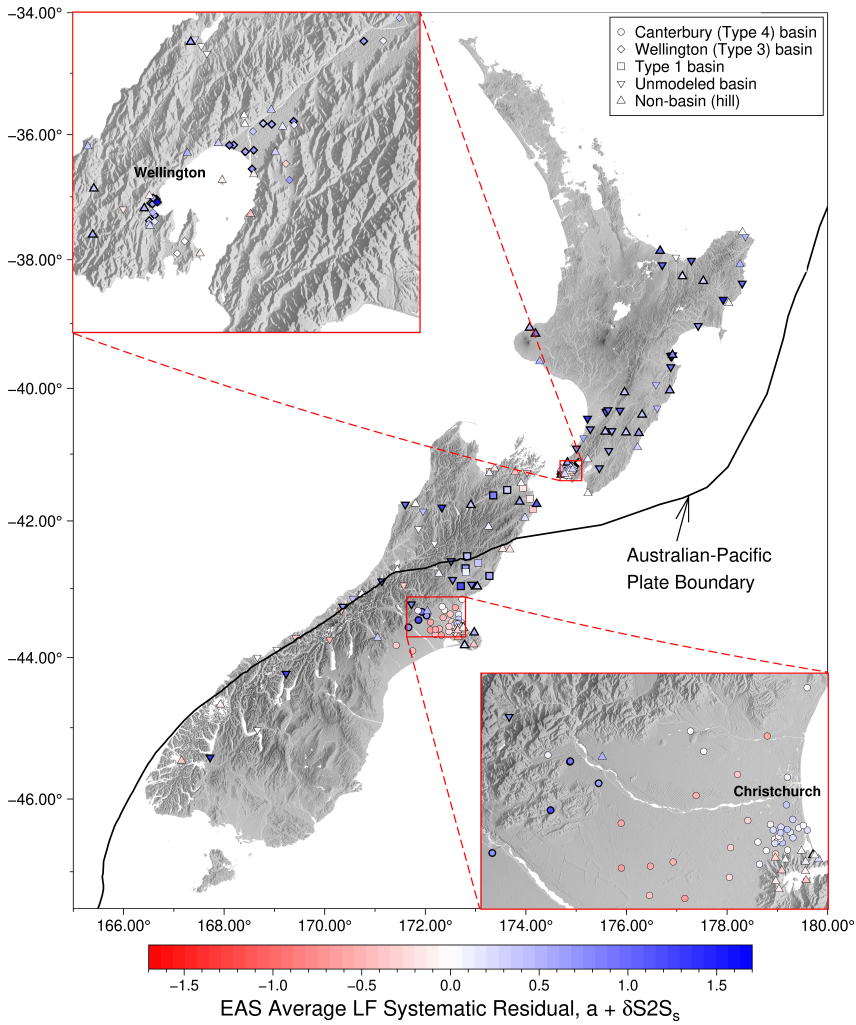

Figure 9. Spatial distribution of average LF systematic residual, computed over the frequency range $0.3 - 1.0$ Hz, for the (HF only) BA18 model. Symbols assigned to each site represent different basin type categories. Symbols with thicker outlines indicate sites where there is a considerable reduction in LF residuals when the LF site factor is applied.

In the case of "Canterbury (Type 4) basin", only 10% of sites require LF adjustment. Within the three categories with the highest proportion of sites benefited by the "LF+HF" approach, it is possible to disaggregate the results by geomorphic categories (Tiwari et al. 2024). Figures 10b, 10c, and 10d display these distributions for the "Unmodeled basin", "Wellington (Type 3) basin", and "Type 1 basin" categories, respectively. These figures

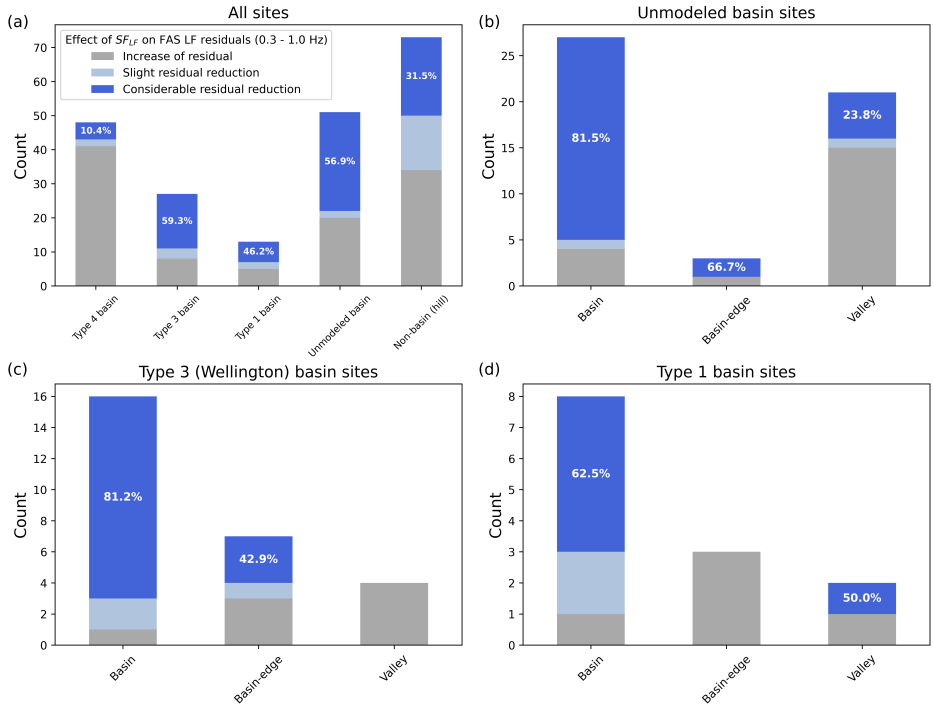

Figure 10. Evaluation of the LF residual reduction obtained by the consideration of SF_{LF} for (a) all sites, (b) unmodeled basin sites, (c) Wellington (Type 3) basin sites), and (d) Type 1 basin sites. In the case of (a), the results are disaggregated by basin-type category, and in the case of (b), (c), and (d), the results are disaggregated by geomorphic category.

show that, by far, the largest proportion of sites benefited by the "LF+HF" approach within these basin type categories correspond to the "Basin" geomorphic category. In contrast, the "Valley" geomorphic category displays a large proportion of sites where the "LF+HF" approach worsens the systematic residuals, which is expected, considering that "Valley" sites are those located within small sedimentary structures (Nweke et al. 2022), where long-period basin effects are less likely to occur. Conversely, "Basin" sites are those located within relatively big sedimentary structures, where large sediment depths and long-period basin effects are more likely. Further dependencies with V_{S30} and $Z_{1.0}$ were examined for each basin-type category, without finding any strong trends (see Figures A.4 and A.5 of the Electronic Supplement A).

Following the above observations, a simple protocol for the application of SF_{LF} was established: SF_{LF} is only applied in the case of sites in the geomorphic category "Basin"

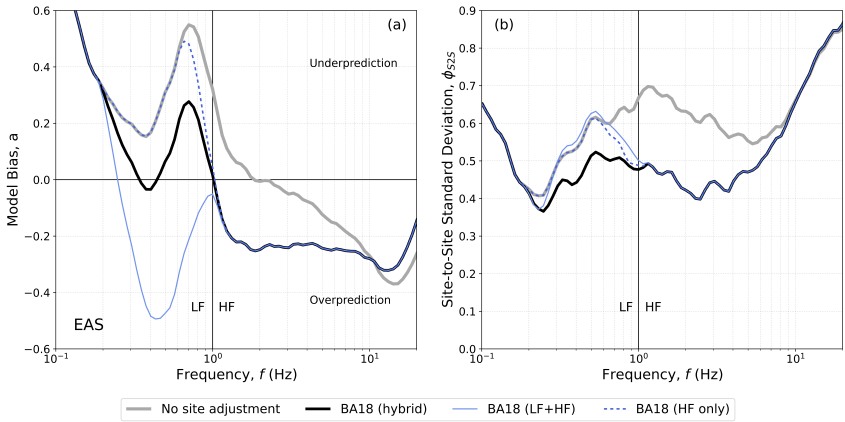

Figure 11. (a) Model prediction bias, a, and (b) site-to-site standard deviation, ϕ_{S2S}, for EAS, considering "no site adjustment", and when the BA18-based SF is applied considering the "hybrid" approach, and when it is applied to both the LF and HF simulation components (i.e., "LF+HF"), and only to the HF simulation component (i.e., "HF only").

that belong to the basin-type categories "Unmodeled basin", "Wellington (Type 3) basin", and "Type 1 basin". This represents 24% of the 212 sites. For the rest of the sites, only SF_{HF} is applied. Figure 11 presents the EAS model bias and site-to-site variability for this "hybrid" SF application approach and compares it to the "HF only" and "LF+HF" approaches (Supplemental Figure A.6 in Electronic Supplement A provides these results disaggregated by basin-type category). As shown, the hybrid protocol results in a significant reduction of the EAS model bias and site-to-site variability in the frequency range $0.3 - 0.8$ Hz. The reduction in variability is up to ≈ 0.1 natural log units for $f = 0.5$ Hz. This is a relevant finding, considering that ground-motion variability can have a significant influence on PSHA computations (e.g., Bommer and Abrahamson 2006; Baker et al. 2021). Supplemental Figure A.7 in Electronic Supplement A shows that for long-period SA, the hybrid approach results in only a slight reduction of the site-to-site variability and even generates some level of overprediction relative to the "HF only" approach. As previously discussed, this is due to the influence of a wide range of FAS frequencies on long-period SA for small-magnitude events (e.g, as illustrated in Figure 7). Figure 11a shows that even with the proposed "hybrid" SF application protocol, the LF simulation component still displays considerable underprediction at some frequencies, which illustrates the limitations of this approach and suggests that further improvements in the basin modeling are required.

Sediment depth consideration

There are multiple V_S profiles that can satisfy a given V_{S30} value, and hence, a range of site responses can be observed at different sites characterized by the same V_{S30}. This illustrates an important limitation of a site factor based solely on one parameter. Even when a site-specific V_S profile is not available, the parameter $Z_{1.0}$ (which is a proxy for sediment depth) can be inferred from regional maps or velocity models (e.g., Wotherspoon et al. 2024), and can be used to differentiate the response of sites with the same V_{S30} but different V_S structures. For example, the BA18 model has a soil depth scaling factor (f_{sed}) that depends on how different $Z_{1.0}$ is from a reference $Z_{1.0}$ value representative of an average site in California conditioned on V_{S30}. This reference model corresponds to the Bayless and Abrahamson (2019) $V_{S30} - Z_{1.0}$ relationship presented in Figure 3.

To incorporate $Z_{1.0}$ into the computation of SF, Equation 3 has to be modified as follows (Kuncar et al. 2025a):

$$SF_1(f) = \frac{\exp(f_{L,actual} + f_{NL,actual} + f_{sed,actual})}{\exp(f_{L,sim} + f_{sed,sim})} \tag{8}$$

where $f_{sed,actual}$ depends on the inferred or measured site-specific V_{S30} and $Z_{1.0}$ values ($V_{S30,actual}$ and $Z_{1.0,actual}$, respectively, corresponding to the best available estimates of the actual parameters), and $f_{sed,sim}$ depends on the values implicit in the simulation ($V_{S30,sim}$ and $Z_{1.0,sim}$, respectively), which can differ for the LF and HF simulation components. Specifically, the LF $V_{S30,sim}$ and $Z_{1.0,sim}$ values are computed from the V_S profile extracted from the NZVM v2.02 at the location of interest, imposing a minimum $V_S = 500$ m/s and 100-m grid spacing. The HF $V_{S30,sim}$ and $Z_{1.0,sim}$ values are computed from the generic V_S profile used in the HF simulation. Supplemental Figures A.8 and A.9 in Electronic Supplement A present a comparison of the 'actual' and (LF and HF) 'simulation' V_{S30} and $Z_{1.0}$ values considered in this study.

To illustrate the modification on the SF that this type of adjustment can produce, Figure 12 shows the adjustment for an example site in Wellington (TEPS site). Figure 12a shows the BA18 reference $V_{S30} - Z_{1.0}$ relationship along with the 'actual' and 'simulation' V_{S30} and $Z_{1.0}$ values for the TEPS site. Due to the relatively shallow depth of the Wellington basin, the 'actual' $Z_{1.0}$ is significantly lower than the typical value for a site in California (Figure 12a). Figure 12b shows the effect that this has on the sediment depth adjustment (expressed as the multiplicative factor $\exp(f_{sed,actual})$) for a frequency of 0.5 Hz (in the LF simulation range), and for 10 Hz (in the HF simulation range). For

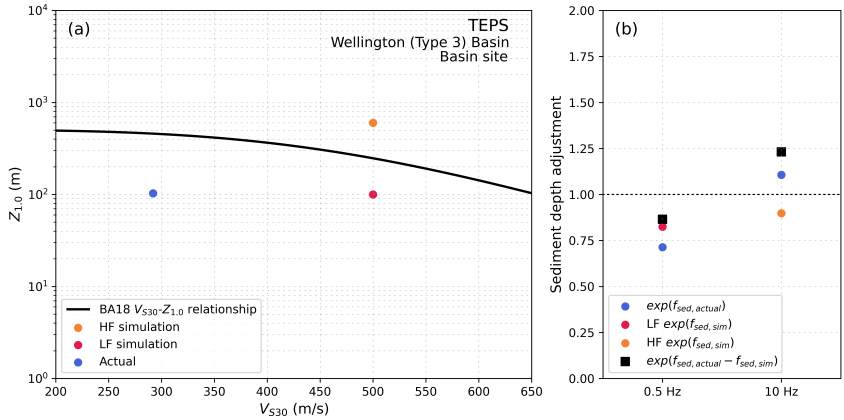

Figure 12. Effect of the incorporation of $Z_{1.0}$ on the site factor, in addition to V_{S30}. (a) $V_{S30} - Z_{1.0}$ relationship considered in the BA18 model, and actual and simulated site parameters considered for the TEPS site. (b) Resulting adjustments to the site factor at 0.5 Hz (LF range) and 10 Hz (HF range).

$f = 0.5$ Hz, $\exp(f_{sed,actual}) < 1$ and for $f = 10$ Hz, $\exp(f_{sed,actual}) > 1$. This means that the 'actual' site-response prediction at TEPS has to be reduced at low frequencies to account for the fact that the basin is shallower than the reference basin considered in the BA18 model, and the opposite is true at very high frequencies. Similarly, the $Z_{1.0}$ value for the LF simulation is below the relationship for California, but is plotted further to the right because the minimum V_S considered in the simulation was 500 m/s (Figure 12a). As a result, the LF $\exp(f_{sed,sim})$ adjustment is less significant than $\exp(f_{sed,actual})$ at 0.5 Hz (Figure 12b). As inferred from Equation 8, the total sediment depth adjustment component of the site factor corresponds to $\exp[f_{sed,actual} - f_{sed,sim}]$, which in this (LF) case is ≈ 0.86, meaning that a 14% reduction in the site factor is obtained when $Z_{1.0}$ is included. In the case of the HF simulation, a generic V_S profile is used for the entire country, which results in a different $Z_{1.0,sim}$ value from that of the LF simulation. The $Z_{1.0,sim}$ value for the HF simulation is above the California relationship, which results in $\exp(f_{sed,sim}) < 1$ and a final adjustment $\exp[f_{sed,actual} - f_{sed,sim}] \approx 1.23$ at 10 Hz.

This $Z_{1.0}$-based "sediment depth" adjustment was applied to the entire database considering the hybrid SF application protocol defined in the "SF application frequency range" section. Figure 13 presents the resulting model bias for EAS, SA, and other IMs considered, obtained with this adjustment and compares it with the case where $Z_{1.0}$ is not considered (Supplemental Figure A.10 in Electronic Supplement A presents the EAS results disaggregated by basin type category). Figure 13a shows that the $Z_{1.0}$-based

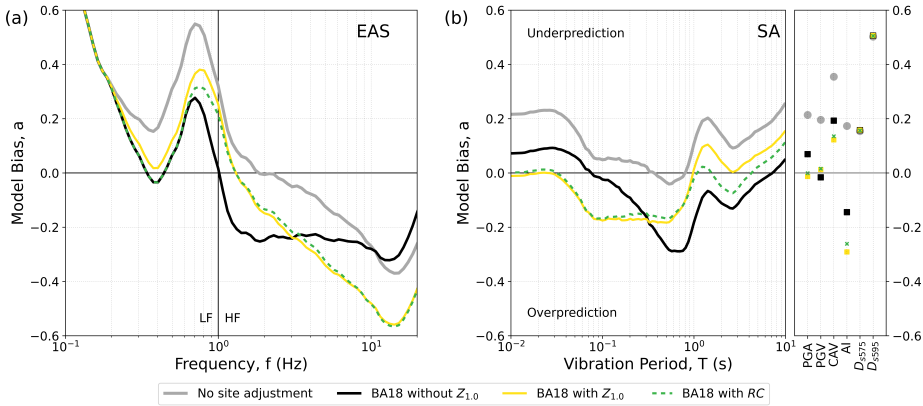

Figure 13. Model bias for (a) EAS and (b) SA and other IMs, considering "no site adjustment" and alternative site factors based on the BA18 model. The application of the site factors is done using the "hybrid" SF application protocol proposed in the "Frequency range of SF application" section. 'BA18 without $Z_{1.0}$' is the conventional V_{S30} site factor SF_1; 'BA18 with $Z_{1.0}$' is the site factor SF_1 incorporating the f_{sed} term; and 'BA18 with RC' corresponds to the application of the reference correction factor (RC) to SF_1 (i.e., SF_2) described in the "Incorporating a host-to-target V_S-profile adjustment" section. In this case, SF_1 is computed without the f_{sed} term.

adjustment allows for a significant reduction of the systematic overprediction of EAS at $f = 1.5 - 3.0$ Hz and SA at $T = 0.3 - 1.0$ s, as well as a reduction of the systematic underprediction of SA at $T < 0.03$. Figure 13a shows that at $f > 3.0$ Hz, the inclusion of the $Z_{1.0}$-based adjustment results in additional overprediction, which was already present before applying any site factor, and this overprediction also manifests for SA at $T = 0.03 - 0.3$ s. (Figure 13b). Figure A.11 in the Electronic Supplement A shows that a slight reduction in SA site-to-site variability is obtained at $T = 0.35 - 0.7$ s when the $Z_{1.0}$-based adjustment is included. It should be noted that this adjustment relies on the "actual" $Z_{1.0}$ values, which in this study present a high level of uncertainty, with only a few sites having values constrained by measurements. Hence, caution should be used when applying this adjustment in future studies.

Incorporating a host-to-target V_S-profile adjustment

Figure 12a showed that the HF $Z_{1.0,sim}$ is above the California relationship, meaning that the HF simulation V_S profile is deeper than the V_S profile implicit in the BA18 model for $V_{S30} = 500$ m/s. A more direct way to correct the site factor to account for these differences is to apply a host-to-target adjustment, using the implicit (host) profile in

the GMM considered (Kamai et al. 2016; Al Atik and Abrahamson 2021) and the HF simulation profile (target profile). This is referred to as "Method 2" in Kuncar et al. (2025a). More specifically, the Method 2 SF (SF_2) is

$$SF_2(f) = \frac{\exp[f_{S,actual}(f)]}{\exp[f_{S,sim}(f)]} \cdot \frac{I_{host(V_{S30,sim})}(f)}{I_{sim}(f)} = SF_1(f) \cdot RC(f) \quad (9)$$

where $I_{host(V_{S30,sim})}$ and I_{sim} are the (impedance-based) site amplifications computed with the square-root-impedance (SRI) method (Joyner et al. 1981; Boore 2013) for the GMM host V_S profile associated with $V_{S30,sim}$ and for the simulation profile, respectively. *RC* is the reference correction factor, which adjusts SF_1.

Figure 14a shows the California Kamai et al. (2016) V_S model (herein, referred to as the K16 model) for $V_{S30} = 500$ m/s and compares it with the HF simulation profile. The K16 model was developed using 553 V_S profiles for stations in California included in the NGA-West2 database (Ancheta et al. 2014). Since the BA18 model was developed for California using the same database, the K16 model can be assumed to represent the host profile for this GMM (following one of the approaches described in Williams and Abrahamson 2021). Al Atik and Abrahamson (2021) showed that the host profile may display considerable variability between GMMs developed using the same database, and hence, it should be noted that there is an important level of uncertainty in the host profile estimate. Figure 14a illustrates significant differences between the host and simulation profiles, which are both characterized by the same $V_{S30} = 500$ m/s. The host profile has a higher V_S at depth, meaning that the site factor assumes a stiffer reference condition than appropriate, which can lead to overamplification (Kuncar et al. 2025a). As explained in Kuncar et al. (2025a), the HF simulation profile is significantly deeper than the host profile because it was artificially truncated to $V_S = 500$ m/s in the shallow part for its implementation in the ground-motion simulation method (e.g., which does not explicitly model soil nonlinearity) but its deeper structure is actually representative of a softer site. Figure 14b shows the resulting *RC*, which indicates that the host-to-target adjustment produces deamplification of the site factor (SF_1) for $f < 3.5$ Hz and amplification at higher frequencies. Figure 14c illustrates the effect of this adjustment in the HF site factor ('BA18 with *RC* adjustment', corresponding to SF_2) for the TEPS site, considering an HF PGA of 0.01 g. Interestingly, the figure shows that for this site, this adjustment has a similar effect to the incorporation of $Z_{1.0}$ investigated in the previous section.

RC was applied to the entire database considering the hybrid SF application protocol defined in the "Frequency range of SF application" section. Due to the higher uncertainty

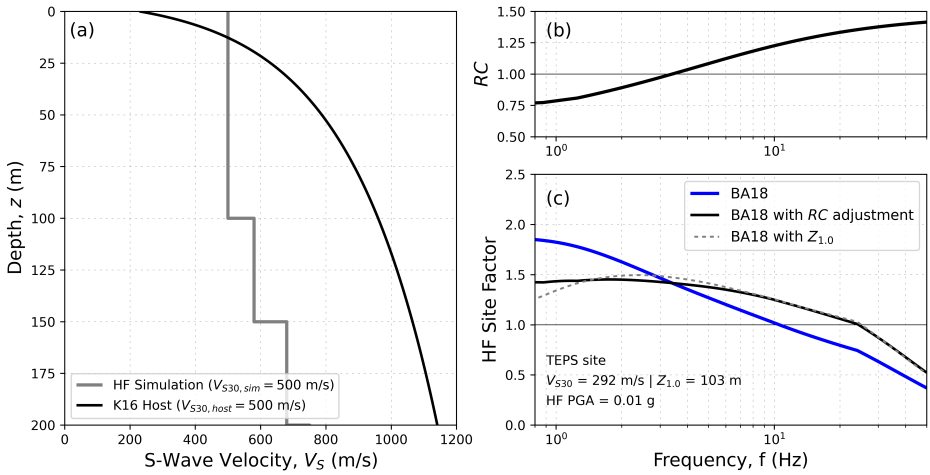

Figure 14. (a) Difference between the HF simulation profile and the host Kamai et al. (2016) profile for California, for a condition of $V_{S30} = 500$ m/s. (b) Resulting reference correction factor, RC, and (c) its effect on the BA18-based SF for the TEPS site.

involved in the estimation of the host profile at greater depths (e.g., the Kamai et al. (2016) velocity model is relatively well constrained only down to $\approx$ 200 m), the application of *RC* was considered only for the HF simulation component. Figure 13 includes the model bias considering *RC*, and shows that the results are very similar to the $Z_{1.0}$-based adjustment previously discussed, with a reduction of the overprediction at $f = 1.5 - 3.0$ Hz and an increase of the overprediction for higher frequencies. It is worth noting that *RC* is only based on the simulation conditions (via the simulation profile and the corresponding host profile), whereas the $Z_{1.0}$-based adjustment modifies both the simulation and actual conditions (via $Z_{1.0,sim}$ and $Z_{1.0,actual}$). These two independent adjustments ($Z_{1.0}$-based and host-to-target adjustments) reduce the peak SA overprediction exhibited at $T = 0.3 - 1.0$ s (for the 'BA18 without Z1.0' case in Figure 13b), suggesting that this overprediction can be explained by differences in the underlying V_S profiles (e.g., HF simulation vs GMM host profile) that are not captured by V_{S30} alone. With the current state of the simulations, which display systematic overprediction at high frequency even before applying the site factor, Figure 13 suggests that these adjustments should be truncated at $f > 3.0$ Hz.

Discussion

Limitations of the V_{S30}-based method and alternative procedure

V_{S30}-based site factors derived from empirical data represent the conventional method for adjusting ground-motion simulations to account for unmodeled site effects, particularly when site-specific data are limited. However, Kuncar et al. (2025a) and the present study highlight that applying these site factors (originally developed for empirical GMMs) to ground-motion simulations can lead to inconsistencies. This was illustrated in Figure 14a, which shows the mismatch between the V_S profile used in the simulation and that implicit in the empirical model for the same V_{S30} value. The host-to-target adjustment investigated here can mitigate this inconsistency, but the accuracy of this procedure may be limited by the high uncertainty in estimating the host profile with current methods.

Kuncar et al. (2025a) examined alternative site-adjustment methods (e.g., Methods 3 and 4) that do not rely on empirical models to predict the linear site response. Instead, they use the SRI method or 1D site-response analysis, and consider the simulation properties as a reference for the site adjustment, ensuring compatibility. Although, in principle, these methods require a site-specific V_S profile, an alternative for their broader application would be to estimate the V_S profile from V_{S30}-based correlations (e.g., Kamai et al. 2016; Shi and Asimaki 2018; Marafi et al. 2021), ideally calibrated for the region of interest. Validation against observations and systematic comparison with the conventional V_{S30}-based method would be needed to establish the appropriate implementation of this approach and assess its benefits.

Conclusions

This article presented a comprehensive investigation on the implementation of V_{S30}-based site factors (SFs) for hybrid broadband ground-motion simulation performed using the Graves and Pitarka (2010, 2015, 2016) method. The analysis was based on validation against observations from 479 small-magnitude events recorded at 212 sites in New Zealand (NZ), resulting in the consideration of 5218 ground motions. Previous validation studies in NZ were focused on intensity measures directly related to engineering applications, such as response spectra (SA) and PGA. In contrast, this study additionally considered the investigation of (Fourier) effective amplitude spectra (EAS) residuals, which allows for a more direct evaluation of the low-frequency (LF) and high-frequency (HF) simulation components. Several aspects related to the implementation of the SF were investigated, including the use of site-response models from alternative

semi-empirical ground-motion models (GMMs), the frequency range of SF application (i.e., whether the site factor should be applied only to the HF simulation component or to both the HF and LF components), the consideration of sediment depth (represented by the parameter $Z_{1.0}$), and the inclusion of a host-to-target V_S-profile adjustment.

Overall, the results showed when the SF is applied to the HF simulation component, the LF simulation exhibits systematic underprediction, and the HF simulation displays systematic overprediction (in terms of EAS). Due to the differences in scaling between Fourier amplitude spectra and SA, the LF underprediction does not manifest at long-period SA, and the HF overprediction is not exhibited for PGA and very short-period SA. The use of site factors based on semi-empirical models for EAS, developed in the last decade, resulted in comparable model bias and variability to response spectra-based models, commonly used in previous validation studies in NZ and other regions. Furthermore, one of the EAS-based models (BA18) allowed for a reduction in the model bias at very high frequencies due to the addition of site attenuation. The systematic biases identified for the entire dataset are considerably less pronounced for the Canterbury basin, corresponding to the higher quality basin model within the 3D velocity model considered in the LF simulation. A stronger low-frequency underprediction was identified at sites located within sedimentary basins less constrained by site data in the 3D velocity model, or that are not properly captured by the spatial discretization used in the finite-difference computation. To address this issue, a simple protocol was proposed to guide the application of the site factor to the LF simulation component. The protocol establishes whether the LF site factor needs to be applied based on the site geomorphic category (Nweke et al. 2022) and the quality of basin representation in the 3D velocity model used for the LF simulation. Specifically, the LF site factor is applied at 'Basin' sites (i.e., those located in the interior of a relatively large sedimentary basin structure) for which the 3D basin model presents some limitations ('Type 3', 'Type 1', or 'Unmodeled basin' categories, in this study). This protocol resulted in the application of the LF site factor at 24% of the 212 sites considered and led to a reduction in EAS prediction variability by up to 0.1 natural log units. Given the physically based rationale that underlies this protocol, it is expected that a similar approach could be suitable for other regions. The incorporation of the parameter $Z_{1.0}$ and the use of a host-to-target correction factor demonstrated that a significant portion of the HF systematic overamplification in the frequency range 1.5-3.0 Hz (manifested strongly for SA in the period range 0.3-1.0 s) can be explained by V_S profile features not accounted for by V_{S30} alone. This includes the particular shape of the simulation profile, which is artificially truncated at the top for the purpose of its

implementation in the simulation method. Due to significant uncertainties in $Z_{1.0}$ and the host profile estimate, further research is needed to establish the best approach to account for these effects in future studies.

This study demonstrated the relevance of properly implementing V_{S30}-based site factors, while also highlighting the limitations of a site adjustment solely based on V_{S30}. The proposed LF SF application protocol represents only an interim solution, and advancements in the characterization and modeling of sedimentary basins across the country should ultimately eliminate the need for a LF site adjustment. This may require considering a finer spatial discretization (i.e., grid spacing < 100 m) in the near-surface, which could be efficiently achieved through the use of a non-uniform grid or by utilizing the Domain Reduction Method (e.g., McCallen et al. 2024; Bielak 2003). For the HF simulation component, some improvements were obtained by properly selecting the GMM and considering additional information beyond V_{S30}, but significant challenges still remain for the modeling of frequencies greater than 3 Hz, which will require the incorporation of further site-characterization data and a site-specific treatment of κ_0. The findings of this article can be used to inform the application of site adjustments in forward applications. Future studies must consider FAS- or EAS-based models for determining the site factor, and continue the investigation of EAS residuals for a broader range of earthquake scenarios, which will lead to further improvements in the source, path, and site-effect modeling in the LF and HF simulation components.

Acknowledgments

The authors thank Robin Lee (University of Canterbury) for providing the observed and simulated ground-motion databases that were considered in this article, and Ayushi Tiwari (University of Canterbury) for sharing the basin-type and geomorphic classification of the seismic stations. We would also like to gratefully acknowledge the New Zealand eScience Infrastructure (NeSI) [nesi00213] and the Korea Institute of Science and Technology Information (KISTI) [KSC-2023-CRE-0459] for the high-performance computing resources provided.

Declaration of conflicting interests

The author(s) declared no potential conflicts of interest with respect to the research, authorship, and/or publication of this article.

Funding

This work was financially supported by the University of Canterbury, QuakeCoRE: The NZ Centre for Earthquake Resilience, Resilience to Nature's Challenges National Science Challenge, the Marsden Fund, and the New Zealand Natural Hazards Commission. This is QuakeCoRE publication number 1073.

Data and resources

Figures were prepared using Python (`https://www.python.org/`), Matplotlib (`https://matplotlib.org/`), PyGMT (`https://pyGMT.org/`), and Inkscape (`https://inkscape.org/`). The New Zealand Velocity Model (NZVM) code is available at `https://github.com/ucgmsim/Velocity-Model`. Linear mixed-effects regression was performed using the lme4 R package (Bates et al. 2015), through the Python library Pymer4 (Jolly 2018), available at `https://github.com/ejolly/pymer4/`. The computation of the SRI-based site amplification for the host-to-target adjustment was performed using the Python library pyStrata (Kottke et al. 2023), available at `https://github.com/arkottke/pystrata`. Site parameters and results are accessible at `https://github.com/felipekuncar/VS30siteFactorValidation/`.

Supplemental material

Supplemental material for this article is available online.

References

Al Atik L and Abrahamson N (2021) A Methodology for the Development of 1D Reference VS Profiles Compatible with Ground-Motion Prediction Equations: Application to NGA-West2 GMPEs. *Bulletin of the Seismological Society of America* 111(4): 1765–1783. DOI:10.1785/0120200312. URL `https://pubs.geoscienceworld.org/bssa/article/111/4/1765/600846/A-Methodology-for-the-Development-of-1D-Reference`.

Ancheta TD, Darragh RB, Stewart JP, Seyhan E, Silva WJ, Chiou BSJ, Wooddell KE, Graves RW, Kottke AR, Boore DM, Kishida T and Donahue JL (2014) NGA-West2 Database. *Earthquake Spectra* 30(3): 989–1005. DOI:10.1193/070913EQS197M. URL `https://journals.sagepub.com/doi/10.1193/070913EQS197M`.

Atik LA, Abrahamson N, Bommer JJ, Scherbaum F, Cotton F and Kuehn N (2010) The variability of ground-motion prediction models and its components. *Seismological Research Letters* 81(5): 794–801. DOI:10.1785/gssrl.81.5.794. URL https://pubs.geoscienceworld.org/srl/article/81/5/794-801/143735.

Atkinson GM (2022) Backbone ground-motion models for crustal, interface and slab earthquakes in New Zealand DOI:10.21420/QMJ6-P189. URL https://shop.gns.cri.nz/sr_2022-11-pdf. Publisher: GNS Science.

Atkinson GM (2024) Constraints on seismological models for NZ crustal earthquakes as obtained from Fourier amplitudes. Technical Report Draft Report to GNS.

Baker J, Bradley B and Stafford P (2021) *Seismic hazard and risk analysis*. Cambridge University Press. ISBN 1-108-57084-4.

Bates D, Mächler M, Bolker B and Walker S (2015) Fitting linear mixed-effects models using lme4. *Journal of Statistical Software* 67(1). DOI:10.18637/jss.v067.i01. URL http://www.jstatsoft.org/v67/i01/.

Bayless J and Abrahamson NA (2019) Summary of the BA18 Ground-Motion Model for Fourier Amplitude Spectra for Crustal Earthquakes in California. *Bulletin of the Seismological Society of America* 109(5): 2088–2105. DOI:10.1785/0120190077. URL https://pubs.geoscienceworld.org/ssa/bssa/article/109/5/2088/573508/Summary-of-the-BA18-GroundMotion-Model-for-Fourier.

Bellagamba X, Lee R and Bradley BA (2019) A Neural Network for Automated Quality Screening of Ground Motion Records from Small Magnitude Earthquakes. *Earthquake Spectra* 35(4): 1637–1661. DOI:10.1193/122118eqs292m. URL https://journals.sagepub.com/doi/10.1193/122118EQS292M. Publisher: SAGE Publications.

Bielak J (2003) Domain Reduction Method for Three-Dimensional Earthquake Modeling in Localized Regions, Part I: Theory. *Bulletin of the Seismological Society of America* 93(2): 817–824. DOI:10.1785/0120010251. URL https://pubs.geoscienceworld.org/bssa/article/93/2/817-824/120872.

Bommer JJ and Abrahamson NA (2006) Why Do Modern Probabilistic Seismic-Hazard Analyses Often Lead to Increased Hazard Estimates? *Bulletin of the Seismological Society of America* 96(6): 1967–1977. DOI:10.1785/0120060043. URL https://pubs.geoscienceworld.org/bssa/article/96/6/1967-1977/146678.

Boon D, Perrin N, Dellow G and Lukovic B (2010) It's Our Fault - Geological and Geotechnical Characterisation and Site Class Revision of the Lower Hutt Valley. Technical Report GNS Science Consulatancy Report 2010/163.

Boore DM (2013) The Uses and Limitations of the Square-Root-Impedance Method for Computing Site Amplification. *Bulletin of the Seismological Society of America* 103(4): 2356–2368. DOI:10.1785/0120120283. URL https://pubs.geoscienceworld.org/bssa/article/103/4/2356-2368/331654.

Boore DM, Stewart JP, Seyhan E and Atkinson GM (2014) NGA-West2 Equations for Predicting PGA, PGV, and 5% Damped PSA for Shallow Crustal Earthquakes. *Earthquake Spectra* 30(3): 1057–1085. DOI:10.1193/070113EQS184M. URL http://journals.sagepub.com/doi/10.1193/070113EQS184M.

Bora SS, Cotton F and Scherbaum F (2019) NGA-West2 Empirical Fourier and Duration Models to Generate Adjustable Response Spectra. *Earthquake Spectra* 35(1): 61–93. DOI:10.1193/110317EQS228M. URL http://journals.sagepub.com/doi/10.1193/110317EQS228M.

Bora SS, Scherbaum F, Kuehn N and Stafford P (2016) On the Relationship between Fourier and Response Spectra: Implications for the Adjustment of Empirical Ground-Motion Prediction Equations (GMPEs). *Bulletin of the Seismological Society of America* 106(3): 1235–1253. DOI:10.1785/0120150129. URL https://pubs.geoscienceworld.org/bssa/article/106/3/1235-1253/332448.

Bradley BA (2013) A New Zealand-Specific Pseudospectral Acceleration Ground-Motion Prediction Equation for Active Shallow Crustal Earthquakes Based on Foreign Models. *Bulletin of the Seismological Society of America* 103(3): 1801–1822. DOI:10.1785/0120120021. URL https://pubs.geoscienceworld.org/bssa/article/103/3/1801-1822/331663.

Bradley BA (2020) Cybershake NZ v19.5: New Zealand simulation-based probabilistic seismic hazard analysis.

Bradley BA, Bora SS, Lee RL, Manea EF, Gerstenberger MC, Stafford PJ, Atkinson GM, Weatherill G, Hutchinson J, De La Torre CA, Hulsey AM and Kaiser AE (2024) The Ground-Motion Characterization Model for the 2022 New Zealand National Seismic Hazard Model. *Bulletin of the Seismological Society of America* 114(1): 329–349. DOI:10.1785/0120230170. URL https://pubs.geoscienceworld.org/bssa/article/114/1/329/631789/The-Ground-Motion-Characterization-Model-for-the.

Bradley BA, Pettinga D, Baker JW and Fraser J (2017a) Guidance on the Utilization of Earthquake-Induced Ground Motion Simulations in Engineering Practice. *Earthquake Spectra* 33(3): 809–835. DOI:10.1193/120216eqs219ep. URL https://journals.sagepub.com/doi/10.1193/120216eqs219ep.

Bradley BA, Razafindrakoto HNT and Polak V (2017b) Ground-Motion Observations from the 14 November 2016 M_{w} 7.8 Kaikoura, New Zealand, Earthquake and Insights from Broadband Simulations. *Seismological Research Letters* 88(3): 740–756. DOI:10.1785/0220160225. URL https://pubs.geoscienceworld.org/srl/article/88/3/740-756/284016.

Bradley BA, Wotherspoon LM, Kaiser AE, Cox BR and Jeong S (2018) Influence of Site Effects on Observed Ground Motions in the Wellington Region from the Mw 7.8 Kaikōura, New Zealand, Earthquake. *Bulletin of the Seismological Society of America* 108(3B): 1722–1735. DOI:10.1785/0120170286. URL https://pubs.geoscienceworld.org/ssa/bssa/article/108/3B/1722/529264/Influence-of-Site-Effects-on-Observed-Ground.

Campbell KW and Bozorgnia Y (2014) NGA-West2 Ground Motion Model for the Average Horizontal Components of PGA, PGV, and 5% Damped Linear Acceleration Response Spectra. *Earthquake Spectra* 30(3): 1087–1115. DOI:10.1193/062913EQS175M. URL http://journals.sagepub.com/doi/10.1193/062913EQS175M.

Campbell KW and Bozorgnia Y (2025) Empirical ground-motion models for horizontal Fourier amplitude spectra from fixed-effects and mixed-effects analyses of the NGA-West2 database. *Earthquake Spectra* : 87552930241312708DOI:10.1177/87552930241312708. URL https://journals.sagepub.com/doi/10.1177/87552930241312708.

Chiou BJ and Youngs RR (2008) An NGA Model for the Average Horizontal Component of Peak Ground Motion and Response Spectra. *Earthquake Spectra* 24(1): 173–215. DOI:10.1193/1.2894832. URL https://journals.sagepub.com/doi/10.1193/1.2894832.

Chiou BSJ and Youngs RR (2014) Update of the Chiou and Youngs NGA Model for the Average Horizontal Component of Peak Ground Motion and Response Spectra. *Earthquake Spectra* 30(3): 1117–1153. DOI:10.1193/072813EQS219M. URL https://journals.sagepub.com/doi/10.1193/072813EQS219M.

de la Torre CA, Bradley BA and Lee RL (2020) Modeling nonlinear site effects in physics-based ground motion simulations of the 2010–2011 Canterbury earthquake sequence. *Earthquake Spectra* 36(2): 856–879. DOI:10.1177/8755293019891729. URL http://journals.sagepub.com/doi/10.1177/8755293019891729.

de la Torre CA, Bradley BA, Lee RL, Tiwari A, Wotherspoon LM, Ridden JN and Kaiser AE (2024) Analysis of site-response residuals from empirical ground-motion models to account for observed sedimentary basin effects in Wellington, New Zealand. *Earthquake Spectra* : 87552930241270562DOI:10.1177/87552930241270562. URL https://journals.

920 sagepub.com/doi/10.1177/87552930241270562.

921 Deschenes MR, Wood CM, Wotherspoon LM, Bradley BA and Thomson E (2018) Development
922 of Deep Shear Wave Velocity Profiles in the Canterbury Plains, New Zealand. *Earthquake*
923 *Spectra* 34(3): 1065–1089. DOI:10.1193/122717EQS267M. URL http://journals.
924 sagepub.com/doi/10.1193/122717EQS267M.

925 Dupuis MR, Lee RL and Bradley BA (2025) Hybrid broadband ground-motion simulation
926 validation of small-magnitude subduction earthquakes in New Zealand (Under Review) .

927 Eberhart-Phillips D, Reyners M, Bannister S, Chadwick M and Ellis S (2010) Establishing a
928 Versatile 3-D Seismic Velocity Model for New Zealand. *Seismological Research Letters* 81(6):
929 992–1000. DOI:10.1785/gssrl.81.6.992. URL https://pubs.geoscienceworld.
930 org/srl/article/81/6/992-1000/143761.

931 Ely GP, Jordan TH, Small P and Maechling P (2010) A VS30-derived near-surface seismic velocity
932 model. San Francisco, CA. URL AbstractS51A-1907.

933 Foster KM, Bradley BA, McGann CR and Wotherspoon LM (2019) A $V_{s\,30}$ Map for New
934 Zealand Based on Geologic and Terrain Proxy Variables and Field Measurements. *Earthquake*
935 *Spectra* 35(4): 1865–1897. DOI:10.1193/121118EQS281M. URL https://journals.
936 sagepub.com/doi/10.1193/121118EQS281M.

937 Galasso C, Zareian F, Iervolino I and Graves RW (2012) Validation of Ground-Motion
938 Simulations for Historical Events Using SDoF Systems. *Bulletin of the Seismological*
939 *Society of America* 102(6): 2727–2740. DOI:10.1785/0120120018. URL https://pubs.
940 geoscienceworld.org/bssa/article/102/6/2727-2740/331596.

941 Geyin M and Maurer BW (2023) U.S. National VS30 Models and Maps
942 Informed by Remote Sensing and Machine Learning. *Seismological*
943 *Research Letters* DOI:10.1785/0220220181. URL https://pubs.
944 geoscienceworld.org/srl/article/doi/10.1785/0220220181/619924/
945 U-S-National-VS30-Models-and-Maps-Informed-by.

946 Graves R (2022) Using a grid-search approach to validate the Graves–Pitarka broad-
947 band simulation method. *Earth, Planets and Space* 74(1): 186. DOI:10.1186/
948 s40623-022-01742-y. URL https://earth-planets-space.springeropen.
949 com/articles/10.1186/s40623-022-01742-y.

950 Graves R, Jordan TH, Callaghan S, Deelman E, Field E, Juve G, Kesselman C, Maechling P,
951 Mehta G, Milner K, Okaya D, Small P and Vahi K (2011) CyberShake: A Physics-Based
952 Seismic Hazard Model for Southern California. *Pure and Applied Geophysics* 168(3-4):
953 367–381. DOI:10.1007/s00024-010-0161-6. URL http://link.springer.com/10.

1007/s00024-010-0161-6.

Graves R and Pitarka A (2015) Refinements to the Graves and Pitarka (2010) broadband ground-motion simulation method. *Seismological Research Letters* 86(1): 75–80. DOI:10.1785/0220140101. URL https://pubs.geoscienceworld.org/srl/article/86/1/75-80/315540.

Graves R and Pitarka A (2016) Kinematic ground-motion simulations on rough faults including effects of 3D stochastic velocity perturbations. *Bulletin of the Seismological Society of America* 106(5): 2136–2153. DOI:10.1785/0120160088. URL https://pubs.geoscienceworld.org/bssa/article/106/5/2136-2153/350935.

Graves RW and Pitarka A (2010) Broadband ground-motion simulation using a hybrid approach. *Bulletin of the Seismological Society of America* 100(5A): 2095–2123. DOI:10.1785/0120100057. URL https://pubs.geoscienceworld.org/bssa/article/100/5A/2095-2123/325180.

Hanks TC and McGuire RK (1981) The character of high-frequency strong ground motion. *Bulletin of the Seismological Society of America* 71(6): 2071–2095. DOI:10.1785/BSSA0710062071. URL https://pubs.geoscienceworld.org/bssa/article/71/6/2071/102118/The-character-of-high-frequency-strong-ground.

Hashash YMA, Harmon J, Ilhan O, Stewart JP, Rathje EM, Campbell KW, Silva WJ and Goulet CA (2018) Modelling of Site Amplification via Large Scale Nonlinear Simulations with Applications to North America. In: *Geotechnical Earthquake Engineering and Soil Dynamics V*. Austin, Texas: American Society of Civil Engineers. ISBN 978-0-7844-8146-2, pp. 523–537. DOI:10.1061/9780784481462.051. URL https://ascelibrary.org/doi/10.1061/9780784481462.051.

Hill MP, Kaiser AE, Wotherspoon LM, Manea EF, Lee RL, de la Torre CA and Bradley BA (2022) 3D geological modelling of Wellington Quaternary sediments and basin geometry DOI:10.21420/TS0B-8A37. URL https://shop.gns.cri.nz/sr_2022-33-pdf. Publisher: GNS Science.

Iwaki A, Maeda T, Morikawa N, Miyake H and Fujiwara H (2016) Validation of the Recipe for Broadband Ground-Motion Simulations of Japanese Crustal Earthquakes. *Bulletin of the Seismological Society of America* 106(5): 2214–2232. DOI:10.1785/0120150304. URL https://pubs.geoscienceworld.org/bssa/article/106/5/2214-2232/350996.

Jolly E (2018) Pymer4: Connecting R and Python for Linear Mixed Modeling. *Journal of Open Source Software* 3(31): 862. DOI:10.21105/joss.00862. URL http://joss.theoj.

org/papers/10.21105/joss.00862.

Joyner WB, Warrick RE and Fumal TE (1981) The effect of Quaternary alluvium on strong ground motion in the Coyote Lake, California, earthquake of 1979. *Bulletin of the Seismological Society of America* 71(4): 1333–1349.

Kaklamanos J, Bradley BA, Thompson EM and Baise LG (2013) Critical Parameters Affecting Bias and Variability in Site-Response Analyses Using KiK-net Downhole Array Data. *Bulletin of the Seismological Society of America* 103(3): 1733–1749. DOI:10.1785/0120120166. URL https://pubs.geoscienceworld.org/bssa/article/103/3/1733-1749/349810.

Kamai R, Abrahamson NA and Silva WJ (2014) Nonlinear Horizontal Site Amplification for Constraining the NGA-West2 GMPEs. *Earthquake Spectra* 30(3): 1223–1240. DOI:10.1193/070113EQS187M. URL http://journals.sagepub.com/doi/10.1193/070113EQS187M.

Kamai R, Abrahamson NA and Silva WJ (2016) VS30 in the NGA GMPEs: Regional Differences and Suggested Practice. *Earthquake Spectra* 32(4): 2083–2108. DOI:10.1193/072615EQS121M. URL http://journals.sagepub.com/doi/10.1193/072615EQS121M.

Kawase H (1996) The Cause of the Damage Belt in Kobe: "The Basin-Edge Effect," Constructive Interference of the Direct S-Wave with the Basin-Induced Diffracted/Rayleigh Waves. *Seismological Research Letters* 67(5): 25–34. DOI:10.1785/gssrl.67.5.25. URL https://pubs.geoscienceworld.org/srl/article/67/5/25-34/142126.

Kottke A, Millen M, Stickler Bot and Subsurfaceiodev (2023) arkottke/pystrata: v0.5.2. DOI:10.5281/ZENODO.7551992. URL https://zenodo.org/record/7551992.

Kuncar F, Bradley BA, de La Torre CA, Rodriguez-Marek A, Zhu C and Lee RL (2025a) Methods to account for shallow site effects in hybrid broadband ground-motion simulations. *Earthquake Spectra* : 87552930241301059DOI:10.1177/87552930241301059. URL https://journals.sagepub.com/doi/10.1177/87552930241301059.

Kuncar F, Bradley BA, de la Torre CA, Rodriguez-Marek A, Zhu C and Lee RL (2025b) Validating alternative methods to account for shallow site effects in hybrid broadband ground-motion simulation of small-magnitude earthquakes in New Zealand. *Submitted to Earthquake Spectra* .

Lee RL, Bradley BA, Ghisetti FC and Thomson EM (2017) Development of a 3D Velocity Model of the Canterbury, New Zealand, Region for Broadband Ground-Motion Simulation. *Bulletin of the Seismological Society of America* 107(5): 2131–2150.

DOI:10.1785/0120160326. URL https://pubs.geoscienceworld.org/bssa/article-lookup?doi=10.1785/0120160326.

Lee RL, Bradley BA, Manea EF, Hutchinson JA and Bora SS (2024) Evaluation of Empirical Ground-Motion Models for the 2022 New Zealand National Seismic Hazard Model Revision. *Bulletin of the Seismological Society of America* 114(1): 311–328. DOI:10.1785/0120230180. URL https://pubs.geoscienceworld.org/bssa/article/114/1/311/630019/Evaluation-of-Empirical-Ground-Motion-Models-for.

Lee RL, Bradley BA, Stafford PJ, Graves RW and Rodriguez-Marek A (2020) Hybrid broadband ground motion simulation validation of small magnitude earthquakes in Canterbury, New Zealand. *Earthquake Spectra* 36(2): 673–699. DOI:10.1177/8755293019891718. URL http://journals.sagepub.com/doi/10.1177/8755293019891718.

Lee RL, Bradley BA, Stafford PJ, Graves RW and Rodriguez-Marek A (2022) Hybrid broadband ground-motion simulation validation of small magnitude active shallow crustal earthquakes in New Zealand. *Earthquake Spectra* : 875529302211092DOI:10.1177/87552930221109297. URL http://journals.sagepub.com/doi/10.1177/87552930221109297.

Marafi NA, Grant A, Maurer BW, Rateria G, Eberhard MO and Berman JW (2021) A generic soil velocity model that accounts for near-surface conditions and deeper geologic structure. *Soil Dynamics and Earthquake Engineering* 140: 106461. DOI:10.1016/j.soildyn.2020.106461. URL https://linkinghub.elsevier.com/retrieve/pii/S0267726120310873. Publisher: Elsevier BV.

Matinrad P and Petrone F (2025) Effect of soft sediments modeling on the seismic response of a 3D mid-rise RC building: high-resolution physics-based ground-motion simulations and empirical factors. *Earthquake Spectra* 41(2): 1247–1271. DOI:10.1177/87552930241288529. URL https://journals.sagepub.com/doi/10.1177/87552930241288529.

McCallen D, Pitarka A, Tang H, Pankajakshan R, Petersson NA, Miah M and Huang J (2024) Regional-scale fault-to-structure earthquake simulations with the EQSIM framework: Workflow maturation and computational performance on GPU-accelerated exascale platforms. *Earthquake Spectra* 40(3): 1615–1652. DOI:10.1177/87552930241246235. URL https://journals.sagepub.com/doi/10.1177/87552930241246235.

McGann CR, Bradley B, Wotherspoon L and Lee R (2021) Basin effects and limitations of 1D site response analysis from 2D numerical models of the Thorndon basin. *Bulletin of the New Zealand Society for Earthquake Engineering* 54(1): 21–30. DOI:10.5459/bnzsee.54.1.21-30. URL https://bulletin.nzsee.org.nz/index.php/bnzsee/article/view/1512.

Nweke CC, Stewart JP, Wang P and Brandenberg SJ (2022) Site response of sedimentary basins and other geomorphic provinces in southern California. *Earthquake Spectra* 38(4): 2341–2370. DOI:10.1177/87552930221088609. URL http://journals.sagepub.com/doi/10.1177/87552930221088609.

Perrin N, Heron D, Kaiser A and van Houtte C (2015) Vs30 and NZS 1170.5 site class maps of New Zealand. Rotorua, New Zealand.

Pilz M, Cotton F and Zhu C (2025) Site-response high-frequency frontiers and the added value of site-specific earthquake record-based measurements of velocity and attenuation. *Earthquake Spectra* : 875529302413113 12DOI:10.1177/87552930241311312. URL https://journals.sagepub.com/doi/10.1177/87552930241311312.

Pitarka A, Graves R, Irikura K, Miyakoshi K and Rodgers A (2020) Kinematic Rupture Modeling of Ground Motion from the M7 Kumamoto, Japan Earthquake. *Pure and Applied Geophysics* 177(5): 2199–2221. DOI:10.1007/s00024-019-02220-5. URL http://link.springer.com/10.1007/s00024-019-02220-5.

Razafindrakoto HNT, Bradley BA and Graves RW (2018) Broadband Ground-Motion Simulation of the 2011 Mw 6.2 Christchurch, New Zealand, Earthquake. *Bulletin of the Seismological Society of America* 108(4): 2130–2147. DOI:10.1785/0120170388. URL https://pubs.geoscienceworld.org/ssa/bssa/article/108/4/2130/532018/Broadband-GroundMotion-Simulation-of-the-2011-Mw62.

Razafindrakoto HNT, Cotton F, Bindi D, Pilz M, Graves RW and Bora S (2021) Regional Calibration of Hybrid Ground-Motion Simulations in Moderate Seismicity Areas: Application to the Upper Rhine Graben. *Bulletin of the Seismological Society of America* 111(3): 1422–1444. DOI:10.1785/0120200287. URL https://pubs.geoscienceworld.org/ssa/bssa/article/111/3/1422/596095/Regional-Calibration-of-Hybrid-Ground-Motion.

Rezaeian S, Stewart JP, Luco N and Goulet CA (2024) Findings from a decade of ground motion simulation validation research and a path forward. *Earthquake Spectra* 40(1): 346–378. DOI:10.1177/87552930231212475. URL https://journals.sagepub.com/doi/10.1177/87552930231212475.

Rodgers AJ, Pitarka A, Pankajakshan R, Sjögreen B and Petersson NA (2020) Regional-Scale 3D Ground-Motion Simulations of Mw 7 Earthquakes on the Hayward Fault, Northern California Resolving Frequencies 0–10 Hz and Including Site-Response Corrections. *Bulletin of the Seismological Society of America* 110(6): 2862–2881. DOI:10.1785/0120200147. URL https://pubs.geoscienceworld.org/ssa/bssa/article/110/6/2862/

589660/Regional-Scale-3D-Ground-Motion-Simulations-of-Mw.

Rodriguez-Marek A, Bommer JJ, Youngs RR, Crespo MJ, Stafford PJ and Bahrampouri M (2021) Capturing epistemic uncertainty in site response. *Earthquake Spectra* 37(2): 921–936. DOI:10.1177/8755293020970975. URL http://journals.sagepub.com/doi/10.1177/8755293020970975.

Semmens S, Dellow G and Perrin N (2010) It's Our Fault - Geological and Geotechnical Characterisation of the Wellington Central Business District. Technical Report GNS Science Consulatancy Report 2010/176.

Seyhan E and Stewart JP (2014) Semi-Empirical Nonlinear Site Amplification from NGA-West2 Data and Simulations. *Earthquake Spectra* 30(3): 1241–1256. DOI:10.1193/063013EQS181M. URL http://journals.sagepub.com/doi/10.1193/063013EQS181M.

Shi J (2019) *Improving Site Response Analysis for Earthquake Ground Motion Modeling*. PhD Thesis, California Institute of Technology. DOI:10.7907/X5NZ-DQ21. URL https://resolver.caltech.edu/CaltechTHESIS:05302019-150220368. Medium: PDF Version Number: Final.

Shi J and Asimaki D (2018) A Generic Velocity Profile for Basin Sediments in California Conditioned on VS30. *Seismological Research Letters* 89(4): 1397–1409. DOI:10.1785/0220170268. URL https://pubs.geoscienceworld.org/ssa/srl/article/89/4/1397/531239/A-Generic-Velocity-Profile-for-Basin-Sediments-in. Publisher: Seismological Society of America (SSA).

Stafford PJ (2014) Crossed and nested mixed-effects approaches for enhanced model development and removal of the ergodic assumption in empirical ground-motion models. *Bulletin of the Seismological Society of America* 104(2): 702–719. DOI:10.1785/0120130145. URL https://pubs.geoscienceworld.org/bssa/article/104/2/702-719/331749.

Stafford PJ (2022) A model for the distribution of response spectral ordinates from New Zealand crustal earthquakes based upon adjustments to the Chiou and Youngs (2014) response spectral model DOI:10.21420/5098-0S19. URL https://shop.gns.cri.nz/sr_2022-15-pdf/. Publisher: GNS Science.

Stafford PJ, Rodriguez-Marek A, Edwards B, Kruiver PP and Bommer JJ (2017) Scenario Dependence of Linear Site-Effect Factors for Short-Period Response Spectral Ordinates. *Bulletin of the Seismological Society of America* 107(6): 2859–2872. DOI:10.1785/0120170084. URL https://pubs.geoscienceworld.org/bssa/

article-lookup?doi=10.1785/0120170084.

Thomson EM, Bradley BA and Lee RL (2020) Methodology and computational implementation of a New Zealand Velocity Model (NZVM2.0) for broadband ground motion simulation. *New Zealand Journal of Geology and Geophysics* 63(1): 110–127. DOI:10.1080/00288306.2019.1636830. URL https://www.tandfonline.com/doi/full/10.1080/00288306.2019.1636830.

Tiwari A, Bradley B, De Torre C, Schill C and Lee R (2024) Nationwide investigation of systematic site effects in New Zealand: Residual analysis of physics-based ground motion simulations. *Japanese Geotechnical Society Special Publication* 10(47): 1741–1746. DOI:10.3208/jgssp.v10.OS-36-01. URL https://www.jstage.jst.go.jp/article/jgssp/10/47/10_v10.OS-36-01/_article.

Van Houtte C, Ktenidou OJ, Larkin T and Holden C (2018) A continuous map of near-surface S-wave attenuation in New Zealand. *Geophysical Journal International* 213(1): 408–425. DOI:10.1093/gji/ggx559. URL https://academic.oup.com/gji/article/213/1/408/4775127.

Walling M, Silva W and Abrahamson N (2008) Nonlinear Site Amplification Factors for Constraining the NGA Models. *Earthquake Spectra* 24(1): 243–255. DOI:10.1193/1.2934350. URL http://journals.sagepub.com/doi/10.1193/1.2934350.

Williams T and Abrahamson N (2021) Site-Response Analysis Using the Shear-Wave Velocity Profile Correction Approach. *Bulletin of the Seismological Society of America* 111(4): 1989–2004. DOI:10.1785/0120200345. URL https://pubs.geoscienceworld.org/bssa/article/111/4/1989/599198/Site-Response-Analysis-Using-the-Shear-Wave.

Wotherspoon LM, Kaiser AE, Stolte AC and Manea EF (2024) Development of the Site Characterization Database for the 2022 New Zealand National Seismic Hazard Model. *Seismological Research Letters* 95(1): 214–225. DOI:10.1785/0220230219. URL https://pubs.geoscienceworld.org/srl/article/95/1/214/629304/Development-of-the-Site-Characterization-Database.